Technical Aspects of Fast Field Cycling

by Gianni Ferrante and Stanislav Sykora
Stelar s.r.l.,Via E. Fermi, 4 I-27035 Mede (PV), Italy; www.stelar.it

CONTENTS

Published in **Advances in Inorganic Chemistry**, Vol. **57**, *Relaxometry of water-metal ion interactions*, Editors Rudi van Eldik R. and Ivano Bertini, Elsevier 2004 (ISBN 0-120-23657-5), pp.405-470.
This draft need not correspond to the final text. Reproduction is permitted for personal use only.

I. Introduction

Since the earliest days of Nuclear Magnetic Resonance (NMR) it has been clear (*1-10*) that relaxation mechanisms were to play an important role in all its applications. In fact, even the first detection of an NMR signal (*11-12*) has been delayed (*12-13*) by several years because the chosen compounds had, unluckily, excessively long relaxation times.

From the pioneering BPP (Bloembergen-Purcell-Pound) formula (*7*), published already in 1948, it became immediately evident that, qualitatively speaking,

- NMR relaxation times, particularly the longitudinal ones, are dependent, through the Larmor frequency, upon the magnetic field induction B_0.
- The relaxation mechanisms require some kind of nuclear interaction subject to stochastic fluctuations, typically due to random molecular motions.
- The most pronounced relaxation phenomena (in terms of field dependence) were to be expected at relatively low fields where low-frequency molecular motions can have a very large impact on the longitudinal relaxation times T_1.

The dependence of $T_1(B)$ on the field B has been soon nicknamed as the *T_1 dispersion curve* or, more recently, Nuclear Magnetic Relaxation Dispersion (*NMRD) profile*. The first experimental curve of this type (Figure 1) has been published in 1950 by Ramsey and Pound (*15,16*).

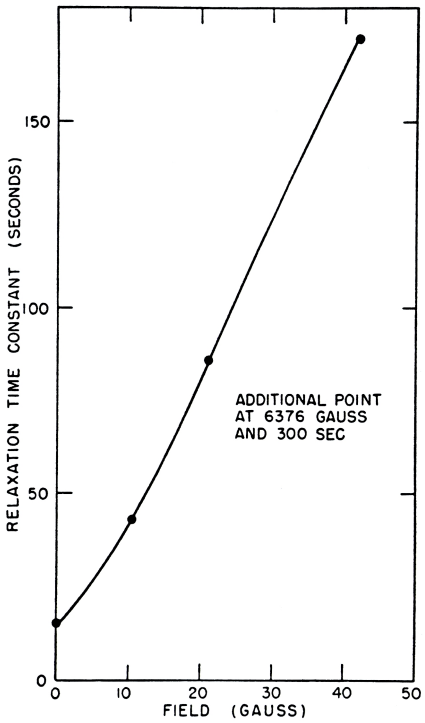

Fig.1. **Relaxation time constant as a function of magnetic field for Li^7 in LiF.**

This very first NMRD profile is reprinted from the article published by Ramsey and Pound (*15*) in 1950.

Published in **Advances in Inorganic Chemistry**, Vol. **57**, *Relaxometry of water-metal ion interactions*, Editors Rudi van Eldik R. and Ivano Bertini, Elsevier 2004 (ISBN 0-120-23657-5), pp.405-470.
This draft need not correspond to the final text. Reproduction is permitted for personal use only.

Many more such curves were measured in subsequent years, some of which were reported by Abragam(*17*). At the time the Abragam's work was published it was already quite clear that the dispersion curves could become a valid tool for the study of *molecular dynamics*, thus laying down the foundations of *variable field NMR relaxometry*. In principal, the dispersion curves are potentially powerful tools for the discrimination between various molecular dynamics models.

The development of this branch of NMR, however, has been quite slow compared to the explosive progress of NMR spectroscopy and, later on, NMR imaging. There are many reasons for this slow start, the most obvious ones being:

- Complexity of NMR relaxation theories (*1,7-9,18-48*).
- Lack and/or complexity of molecular dynamics models.
- Practical difficulties inherent in measuring the dispersion curves.

Since this is essentially an engineering paper, we shall dwell only on the last point. Already from the BPP formula it was qualitatively clear that, in order to become efficient and useful tools, the dispersion curves must extend over a wide interval of relaxation field values (preferably several orders of magnitude).

Achieving this goal using the traditional, fixed-field approach was almost impossible. One can, of course, use an electromagnet and a broad-band NMR console and, re-tuning the system at every point of the measured profile, carry out a conventional relaxation time measurement at many field values. Apart from being painfully slow, however, such an approach is limited to at best one decade of rather high field values. At fields corresponding to less than about 1 MHz of ^{1}H Larmor frequency, the signal excitation and detection technologies in fact change too much to use the same type of instrument and, in addition, the signal becomes often too weak to be detected.

Limited fixed-field, traditional relaxation measurements at very low fields, including the Earth field, were of course carried out (*49*) using specially build NMR systems. Such measurements confirmed the general tendency of relaxation times to be more 'discriminating' at low fields than at high fields. The fact has been even used to produce a medical low-field NMR system capable of diagnosing particular fetal pathologies by means of in-vivo measurements of the longitudinal relaxation time of the amniotic liquid. Even such systems, however, were limited to a quite narrow relaxation field interval.

It became clear very soon that in order to cover comfortably a wide range of relaxation field values, one had to use an excitation/detection assembly operating at some fixed field and, during the relaxation periods of a relaxation-measurement NMR sequence, subject the sample to another, easily variable field. One rather obvious solution for such an arrangement was to combine a fixed field, conventional NMR relaxometer operating at a high field with an auxiliary variable electromagnet and, during the sequence, *mechanically shuttle* the sample between the two magnetic fields.

For almost three decades, many T_1 dispersion curves (including the first one shown in Figure 1) were actually measured by moving the sample manually from one magnet to the other. Quite soon, however, mechanical devices (*50-64*) have been developed to achieve the task, some of which were quite sophisticated.

Since, during an actual measurement, the shuttling process is repeated many times in a cyclic manner, the technique has been named *field-cycling (FC) NMR relaxometry*, a term which

Published in **Advances in Inorganic Chemistry**, Vol. **57**, *Relaxometry of water-metal ion interactions*,
Editors Rudi van Eldik R. and Ivano Bertini, Elsevier 2004 (ISBN 0-120-23657-5), pp.405-470.
This draft need not correspond to the final text. Reproduction is permitted for personal use only.

underlines the fact that it is the *magnetic field variation* that matters and not the manner in which it is achieved.

The main drawback of mechanical shuttling consists in the relatively long time needed to move the sample physically between the two fields. Even with the best devices, there are severe limits on the maximum acceleration/deceleration, dictated by the mechanical stability of the sample transport system as well as of the sample. Consequently, relaxation times much shorter than 100 ms (R_1 above 10) are almost impossible to measure, ruling out an enormous segment of potentially interesting applications. On the other hand, mechanical shuttling systems had been successfully combined with high-field, high-resolution NMR spectroscopy (*64*), a feature which is still quite unique.

Starting in the early 70's, a new approach began to take hold, consisting in keeping the sample fixed while the field, produced by an air-core electromagnet, is being switched between different field values. This approach, named *fast field-cycling (FFC) NMR relaxometry*, explored primarily by Redfield *(35,75)* Noack *(61,65,67,77)* Koenig *(58,66,78)* and Kimmich *(61,73,76,77,94)* has the potential of handling much faster relaxing samples (the current upper limit of manageable R_1 is between 1000 and 10000, depending upon the shape of the NMRD profile). It requires a novel type of magnets and power supplies, the development of which is still in progress.

The advent of the FFC instruments has opened a number of important application areas (molecular dynamics of liquid crystals, paramagnetic contrast MRI agents, proteins, polymers, etc) and thus provided a powerful impulse for further development of variable-field NMR relaxometry. Since 1996, Stelar entered the field and, building on the Noack-Schweikert technology (*67*), started producing the first commercial FFC NMR relaxometers. The availability of such instruments has further enhanced the drive towards new applications, apart from confirming the enormous potential of the technique as a primary tool for the study of molecular dynamics of even quite complex systems.

In what follows, we wish to describe the most important technical aspects of Fast Field Cycling NMR relaxometry, including both the required special hardware (magnet, power supply, etc.) and the measurement methodology (data acquisition sequences and, to some extend, the subsequent data evaluation). Naturally, the description shall be based primarily on our own experience which has not yet been described in detail elsewhere.

II. Premises of FFC NMR relaxometry

In a conventional NMR instrument the resonant magnetic induction of a nuclide immersed in a field with magnetic induction B occurs at the Larmor frequency $\omega_L=\gamma B$, where γ is the nuclide's gyromagnetic ratio. Since the NMRD profiles should cover several orders of magnitude of the field value B, they necessarily include sections with very low B values.

Unfortunately, the detection of the signals induced by a given nuclide becomes more and more difficult when B becomes small because of the progressive decrease of the signal to noise ratio (S/N). It is often quoted that the sensitivity decreases with square of the field or, according to more realistic estimates (*65,68*), with factors such as $B^{3/2}$ *or* $B^{7/4}$. The use of field-cycling measurement methods (for details, see Section VIII) is a truly neat way of avoiding all the problems of low-field NMR and allows one to measure relaxation rates over something like five decades of the relaxation field magnitudes without ever changing the RF excitation and detection

Published in **Advances in Inorganic Chemistry**, Vol. **57**, *Relaxometry of water-metal ion interactions*, Editors Rudi van Eldik R. and Ivano Bertini, Elsevier 2004 (ISBN 0-120-23657-5), pp.405-470.
This draft need not correspond to the final text. Reproduction is permitted for personal use only.

hardware!! In principle, it makes it even possible to measure relaxation rates in zero field which would be completely impossible to do in any other way.

A field-cycling experiment requires that the sample be subject at different times, and for variable durations, to different values of the magnetic field B. From the instrumental point of view, there are basically just two ways to achieve this goal.

The first method consists in mechanical translation of the sample between areas with different field intensities (*15,16,50-64*). However, such mechanical "shuttling" methods are inherently slow. It follows that they are applicable only to samples with long relaxation time, limited essentially by the shortest possible time it takes to move the sample from one position to another which is typically about 50 ms.

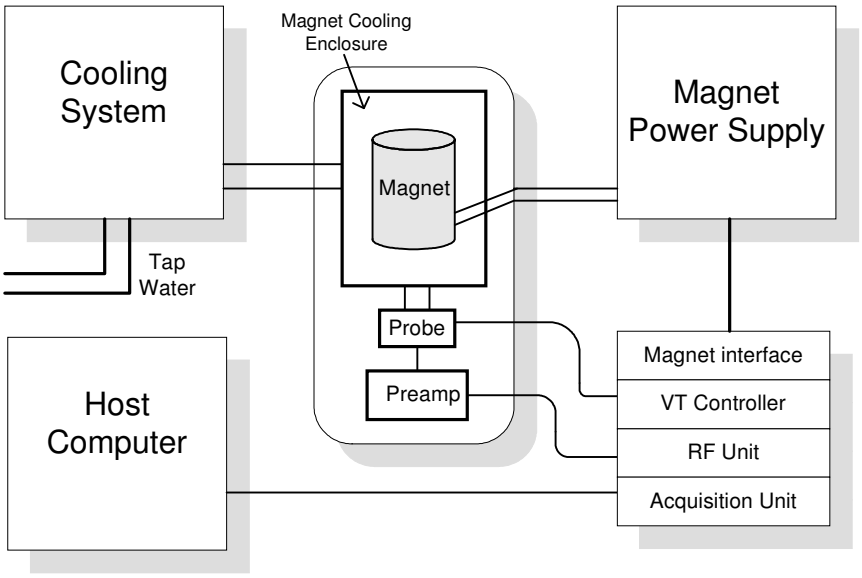

Fig. 2. **Basic block diagram of a FFC NMR Relaxometer**

The second field-cycling method (*65-67*) uses electronic modulation of the current flowing through the coil of an electromagnet. This technique, commonly called Fast Field Cycling (FFC) NMR relaxometry, permits much faster variations of the field induction and thus extends the applicability of the field cycling approach to very short relaxation times T_1, at present down to fractions of a millisecond.

The instrumental aspects which shall be discussed in the following Sections regard primarily the fundamental characteristics and the functional behavior of those parts of an FFC NMR relaxometer which are characteristic of the FFC technique (Figure 2) Subsequently shall be discussed also some of the methodological aspects of FFC NMR relaxometry, such as different data acquisition sequence and data accumulation and evaluation methods.

Above all, the Authors wish to share the experience they have acquired during the development of a commercial series of routine and research FFC NMR relaxometers.

Published in **Advances in Inorganic Chemistry**, Vol. **57**, *Relaxometry of water-metal ion interactions*, Editors Rudi van Eldik R. and Ivano Bertini, Elsevier 2004 (ISBN 0-120-23657-5), pp.405-470.
This draft need not correspond to the final text. Reproduction is permitted for personal use only.

III. The FFC magnet

III A. General considerations

Any NMR field-cycling (FC) relaxometry experiment presumes that the sample is subject to a magnetic field of various intensities for time intervals of varying durations. More specifically, between the various intervals of a relaxation-time measurement, the external *magnetic field induction* B (the Zeeman field) must be made to commute rapidly between several predefined values, such as the polarization field B_p, the relaxation field B_r and the acquisition field B_a.

These values belong to the most important parameters of the experiment and their total range is given by the electric characteristics of the apparatus. The time interval required to commute, or *cycle* between the different field levels is usually called *switching time*. The minimum switching time values depend upon the desired size of the field jump ΔB, defined by the experiment, as well as on the electrical characteristics of the magnet (primarily its inductance and resistance) and of the power supply (primarily its maximum voltage). The latter factors, in fact, define the maximum field-variation rate (i.e., the *slewing rate* s = dB/dt) of an electromagnet, an aspect which shall be discussed in detail in Section IV.C. Evidently, one of the prerogatives of FC relaxometry is to keep the switching times of magnetic fields as short as possible, in principle much shorter than the relaxation rates T_1 of the sample we want to measure. For the sake of completeness, one should mention also the fact that there exist very special situations in which extremely high slewing rates may be undesirable. In particular, this regards relaxation time measurements in extremely low fields where transversal components of Earth and environmental fields may interfere in a manner which depends upon whether the field switching is adiabatic (Larmor periods much shorter than switching times) or non-adiabatic(Larmor periods comparable to switching times). Detailed analysis of such phenomena, however, is beyond the scope of this exposition. *(70)*

From the above it follows that the geometry of an FFC electromagnet must be carefully studied taking into account not just the maximum field B_{max} but also the maximum slewing rate $(dB/dt)_{max}$ achievable with a given power supply. Optimization of both B_{max} and $(dB/dt)_{max}$ leads to the necessity of a compromise, whose resolution defines the final specifications of an FFC magnet (naturally, the compromise must include also another aspect of the problem, as the maximum electrical power, and all technological limits and manufacturing constraints).

III. B. Optimal configuration of an FFC magnet.

A traditional electromagnet with a ferromagnetic yoke would be totally inadequate for FFC experiments since its design aims at the maximization of the field, while no attention is being paid to the slewing rates which turn out to be extremely low. The high inductance values of such magnets are achieved exploiting the very high magnetic permeability μ of ferromagnetic materials. At room temperature, the relative permeability μ/μ_0 is, for example, about 1200 for pure iron, 1300 for cobalt and 400 for nickel (the values for special alloys can be substantially higher). Since field induction $B=\mu H$ is directly proportional to μ, while the magnetic intensity H is given only by the total energization current, high values of μ make it possible to efficiently minimize the electric power needed to produce a given field. On the other hand, the same fact implies an extremely high magnet inductance L. As a result, the typical inductance values of iron-based electromagnets (1-10 Henry) make them unsuitable for field-cycling experiments. To drive

Published in **Advances in Inorganic Chemistry**, Vol. **57**, *Relaxometry of water-metal ion interactions*, Editors Rudi van Eldik R. and Ivano Bertini, Elsevier 2004 (ISBN 0-120-23657-5), pp.405-470.
This draft need not correspond to the final text. Reproduction is permitted for personal use only.

such inductive loads at speeds characteristic of FFC experiments, in fact, the produced over-voltages V = -L(dI/dt) would be enormous, implying extremely costly and complex high-voltage power supplies.

In general, in order to be able to achieve high slewing rates, one has to keep the magnet inductance L reasonably low which, on the other hand, means that the current required to achieve a desired value of B is going to be rather larger (hence the necessity to find a suitable compromise).

Despite the above objections to iron-based magnets, a limited use of materials with high magnetic permeability μ might still be advantageous in the design of low-inductance FFC magnets. It might permit, for a given value of L, to construct magnets with large useful volume and/or lower the required power. Unfortunately, the presence of such materials leads to a number of design and employment problems. Ferrites, for example, exhibit a rather large hysteresis which complicates the management of measurement cycles. Metallic ferromagnets, such as soft iron or Alnico, have a rather limited frequency response since their magnetization involves a reorientation (rather than re-magnetization) of elementary domains. In both cases, moreover, the permeability has a strong temperature dependence which constitutes an additional source of magnetic field instabilities.

Several special electromagnet configurations described in the literature *(79-83)* have characteristics which, theoretically, might be compatible with FFC requirements. However, considering the above objections, it's safe to claim that, at present, the configuration most suitable for FFC NMR relaxometry is a cylindrical magnet composed of one or several coaxial air-core solenoids.

Such a configuration permits to reach elevated maximum field values B_{max} with acceptable slewing rates dB/dt. On the other hand, it presents also a number of design problems and some practical disadvantages.

One of the disadvantages consists in the fact that in axial magnets it is rather difficult to use probes with solenoid RF coils. The difficulties are related to sample insertion/removal complications and to numerous spatial constraints, exacerbated by the presence of a glass dewar for sample-temperature control (see Section VI). This is unfortunate because the alternative saddle coils are substantially less efficient, especially at the relatively low excitation/detection frequencies used in FFC NMR.

The magnet design problems are mostly related to the fact that in any real solenoid the field inhomogeneity ΔB/B at its center is completely insufficient for NMR experiments as to reach the required homogeneity in a simple solenoid, its length-to-diameter ratio would have to be extremely large. Consequently, in a cylindrical magnet, it is always necessary to adopt special designs which optimize field homogeneity over the whole sample volume at the center of the magnet.

One of the simplest and most direct approaches is to modulate the current density distribution along the solenoid *(85-97)*. A suitable longitudinal current density distribution can be obtained by varying the gaps between the loops or by adding special correction coils at the extremes of the solenoid or, as shall be described later, by varying the cross-section of the individual loops. All these methods aim at reducing the length of the solenoid without an excessive degradation of field homogeneity at its center.

Published in **Advances in Inorganic Chemistry**, Vol. **57**, *Relaxometry of water-metal ion interactions*, Editors Rudi van Eldik R. and Ivano Bertini, Elsevier 2004 (ISBN 0-120-23657-5), pp.405-470.
This draft need not correspond to the final text. Reproduction is permitted for personal use only.

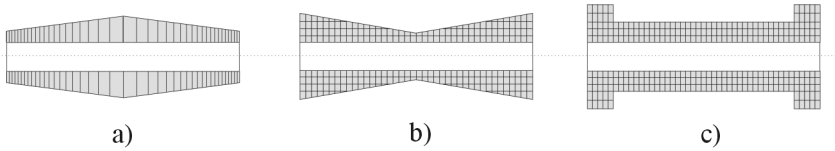

Fig. 3. **Modulation of magnetic flux density B along the axis of an solenoid.**

The figure shows three examples of how one can modulate the density of the current I along the axis of an solenoid and thus indirectly modulate the magnetic field B along its axis a) Graduated current density b) Linear varied winding density c) Outer notch

III. C. Electric and geometric parameters determining maximum B and dB/dt

Consider a cylindrical magnet formed by a simple solenoid with dimensions defined by the inner radius r_0 (half the bore), outer radius r_1 and length $2l$ as the one shown in Figure 4. We shall assume that the magnet has ohmic resistance R and an inductance L and that we pass through it a variable current I which leads to corresponding variation of the magnetic field induction B at its center. In order to do that, we shall use a power supply with an output voltage V, controlled so as to guarantee the desired current *I* (we shall see later the conditions under which this can be done).

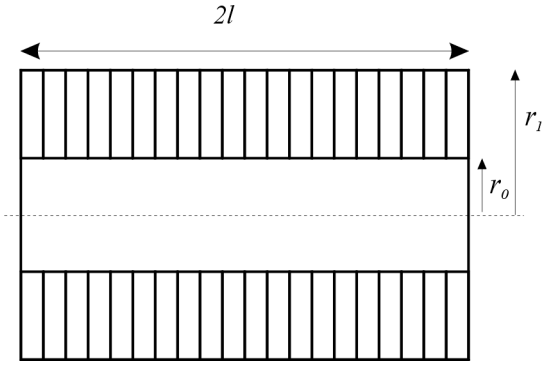

Fig. 4. **Cross section of a simple solenoid**

According to Ampere's law, for any magnet which does not contain ferromagnetic materials, there is a linear dependence between the current I and the central field B. In the case of a thin layer solenoid with $r_0 = r_1 = r$, the relationship is:

$$B = \mu H = \mu \frac{n}{l}\left[1+\left(\frac{r}{l}\right)^2\right]^{-1/2} I \,, \qquad (1)$$

where μ is the magnetic permeability of the medium (in our case $\mu_{air} \approx \mu_0 = 4\pi \times 10^{-7}$ [Vs/Am]), *l* and *n* are length and number of turns of the solenoid.

For a real coil of the type shown in Figure 4 , the magnetic field B can also be expressed with the following equation:

$$B = G\sqrt{\frac{Pf}{\rho_0 r_0}} \qquad (2)$$

Published in **Advances in Inorganic Chemistry**, Vol. **57**, *Relaxometry of water-metal ion interactions*, Editors Rudi van Eldik R. and Ivano Bertini, Elsevier 2004 (ISBN 0-120-23657-5), pp.405-470.
This draft need not correspond to the final text. Reproduction is permitted for personal use only.

which better highlights the relations between electrical power and geometric parameters and geometric shape for a cylindrical coil *(71).*

In equation (2) P is the electrical power applied to the magnet while G is a coefficient, known as the Fabry factor, which depends exclusively upon the normalized geometry of the magnet (for example, in the case represented by Figure 4, G depends only on the ratios r_1/r_0 and l/r_0).

For such a cylindrical solenoid, the typical value of the G factor ranges from a minimum of 0.18 (for an uniform distribution of currents I), up to 0.22 depending on shape of current distribution along the axis of the solenoid.

Notice the non-linear dependence between the field B and the power P required to generate it which, in fact, grows with the square of B.

The coefficient ρ_0 in Eq.(2) defines the resistivity of the solenoid conductor. It is evident that decreasing the resistivity one linearly decreases the power required to generate a given field. Hence, the quantitative advantage of using metals with the lowest possible resistivity. The solenoid bore r_0 also affects very strongly the generated field inductance B. Though it is not directly evident from Eq.(2), other *relative* dimensions of the magnet (i.e., its form as opposed to its dimension) affect B only though the Fabry factor and that dependence is relatively modest.

The factor f , known as the *packing factor*, expresses the ratio between the total conducting volume and the total magnet volume. It should be kept as high as possible, provided that the magnet design minimizes efficiently the isolating gaps between individual winding loops.

Equations (1) and (2) describe the dependence between the current (or power) and the generated field. This direct relationship is inherently independent of any variation of the current. When the current I is made to vary at a rate dI/dt, however, it induces across the magnet an over-voltage L(dI/dt) which needs to be compensated using part of the applied power supply voltage V. In other words, the voltage V across the magnet is composed of two terms, one used to overcome the ohmic resistance (RI) and one to overcome the magnet inductance (L dI/dt). For future convenience, we express the situation by means of the following linear differential equation:

$$\frac{dB_0}{dt} \approx \frac{dI}{dt} = \frac{V - IR}{L} . \qquad (3)$$

One must also bear in mind that the inductance L is, in general, a complex function of the magnet geometry. In the case of a thin-layer solenoid, for example,

$$L = \mu \frac{n^2 \pi \ r^2}{l} \qquad (4)$$

Equations (1)-(4) are used here essentially to illustrate the intricate interdependence between the maximum achievable field, the employed electric power, the maximum slewing rate dB/dt and the geometric parameters of the solenoid. A detailed, quantitative treatment (which must necessarily be carried out when designing an actual magnet) is beyond the scope of this review since, for example, the calculation of G and L for a real magnet is quite complex and requires numerical methods.

Published in **Advances in Inorganic Chemistry**, Vol. **57**, *Relaxometry of water-metal ion interactions*,
Editors Rudi van Eldik R. and Ivano Bertini, Elsevier 2004 (ISBN 0-120-23657-5), pp.405-470.
This draft need not correspond to the final text. Reproduction is permitted for personal use only.

Analyzing Equations (2) and (3), one can show that:

- When B and dB/dt are optimized independently, their maxima are not reached with the same design parameters of the magnet.

- The design parameters therefore always represent a compromise between the maximum achievable field and satisfactory slewing rates. The compromise can be resolved once one has defined the maximum available power, the basic geometry of the solenoid (in particular its volume) and any optimization constraints (see the next point).

- The optimization procedure must keep into account constraints such as maximum admissible local power dissipation and maximum tolerable magnetic field inhomogeneity. In this way, such constraints influence, often quite seriously, the final performance of the magnet.

III D. Example of a real 1Tesla FFC magnet.

We have seen that magnets for FFC NMR experiments should be designed in a way to obtain, for an a-priori given maximum electric power *P*, the highest possible field B, a satisfactory homogeneity B/ΔB over a defined volume and high slewing rates *dB/dt* (this implies low values of the magnet inductance L), under a number of constraints of which the most important ones are the effective sample volume, an upper limit to maximum local power dissipation (the hot spot limit) and, last but not least, reasonably easy manufacturing. All these requirements are strongly interrelated and the systematic optimization of coil geometry is a difficult problem.

A numerical optimization procedure which keeps track of all these factors has been published by Schweikert, Krieg and Noack *(67)*. The algorithm used in this procedure is almost unique; as far as we know, there is only onealternative published by Kimmich *et al.* (73) that achieves a similar degree of completeness.

We have found the Noack-Schweikert approach very advantageous. Once we had mastered the rather complex cutting and assembly technology, we used it with excellent results to develop commercially available magnets for FFC NMR relaxometers with maximum field from 0.5 T up to 1 T *(72)*

***Fig. 5*. Example of a solenoid of the Noack-Schweikert type**

The cylindrical configuration of a Noack-Schweikert type foresees the use of several coaxial solenoids connected electrically so that their individual fields are summed together. The winding of each solenoid is realized by cutting a variable-step spiral in a thick-walled metal cylinder (Figure 5). The slope of the spiral along the magnet length is continuously varied according to a

Published in **Advances in Inorganic Chemistry**, Vol. **57**, *Relaxometry of water-metal ion interactions*,
Editors Rudi van Eldik R. and Ivano Bertini, Elsevier 2004 (ISBN 0-120-23657-5), pp.405-470.
This draft need not correspond to the final text. Reproduction is permitted for personal use only.

pre-calculated, optimized function. In this way the thickness of the individual winding loops varies in a way which optimizes the current distribution.

The mathematical formalism used to calculate the best current distribution consists of a numeric inversion of the Biot-Savart differential relations between field and current for a given geometric configuration of the conductive loops. At the same time, all imposed constraints are being taken care of by means of the standard Lagrange formalism.

Having fixed the basic geometry and the required power, the algorithm looks iteratively for the current density distribution which maximizes the generated field while maintaining the necessary field homogeneity over a pre-defined volume.

In a refined form, this design method has been used by Stelar to develop and manufacture FFC magnets, commercially available since 1997. In what follows we shall discuss in more detail some of the practical aspects of this design approach when applied to the development of a 1T magnet optimized for the highest Fabry factor and the highest slewing rates compatible with current technology..

The first task in a Noack-Schweikert magnet design is the definition of the best initial set of parameters and constraints, such as the number and dimensions of individual solenoids (layers), the maximum electrical power to be used and the best materials. To define these parameters, one must consider numerous limitations arising from the manufacturing technology as well as the performance characteristics of the cooling system and of the power supply. In fact, magnet cooling efficiency leads to one of the most stringent limits to using ever higher electric power. Moreover, because of finite manufacturing tolerances and other technological problems, the magnetic field homogeneity obtained in practice is quite far from the calculated theoretical values.

In principle, one could consider a number of metals and alloys to be used for the construction of the magnet but, considering their physical and electrical characteristic, copper and silver are undoubtedly the best choices. This assertion sounds obvious but the use of other metals with higher resistivity, such as aluminum alloys, is sometimes justified because of their negligible cost and mechanical properties which simplify the manufacturing process. The most important physical characteristics of the best conductors such as OF copper (Oxygen Free) and silver, are shown in Table I .

Table I. Main physical parameters of copper and silver in SI units

	Resistivity ρ	**Temperature coefficient α**	**Thermal conductivity σ**	**Mechanical cutting**
Copper OF	1.78×10^{-8}	0.0068	383	Very difficult
Silver	1.58×10^{-8}	0.0061	419	Difficult

Notes: Resistivity is in [Ω.m], its relative temperature coefficient $\alpha = (d\rho/dT)/\rho$ is in K^{-1} and thermal conductivity σ is in $W.m^{-1}.K^{-1}$.

Apart from its higher costs and difficulties to obtain suitably dimensioned silver tubes or cylinders from commercial sources, silver is certainly the most favorable choice since it is

Published in **Advances in Inorganic Chemistry**, Vol. **57**, *Relaxometry of water-metal ion interactions*, Editors Rudi van Eldik R. and Ivano Bertini, Elsevier 2004 (ISBN 0-120-23657-5), pp.405-470.
This draft need not correspond to the final text. Reproduction is permitted for personal use only.

superior to copper in all comparison parameters. It is also worth mentioning at this point that gold, while better than aluminum, is substantially worse than both copper and silver.

On the basis of Eq.(2), it is evident that the lower silver resistivity proportionally reduces the electrical power required to produce a given field. At the same time, it reduces the time constant R/L of the magnet which is an important factor in minimizing the final field-switching times. Section IV C discusses how the magnet time constant R/L and the power supply output voltage affect the maximum achievable slewing rate *dB/dt*).

The lower temperature coefficient and the higher thermal conductivity of silver contribute to improve the final field stability of the system. In fact, the geometrical dimensions of the magnet layers change with the temperature of the metal, because of its thermal dilatation, and thus modify its geometry, causing undesired thermal drifts of the field and, to a lesser extent, even some field homogeneity degradation. The variations of the field B with magnet temperature are not negligible and, when not corrected by suitable countermeasures discussed in Sections IV.D and XI.A, can affect the precision of relaxation rate measurements.

Our choice of the metal for the 1 T magnet was silver. Cutting of the magnet layers from silver tubes was done by means of a specially designed, numerically controlled tooling machine (Figure 6). Traditional tooling machines in fact do not have all the degrees of freedom required to cut a variable-slope spiral in a thick-walled cylindrical tube.

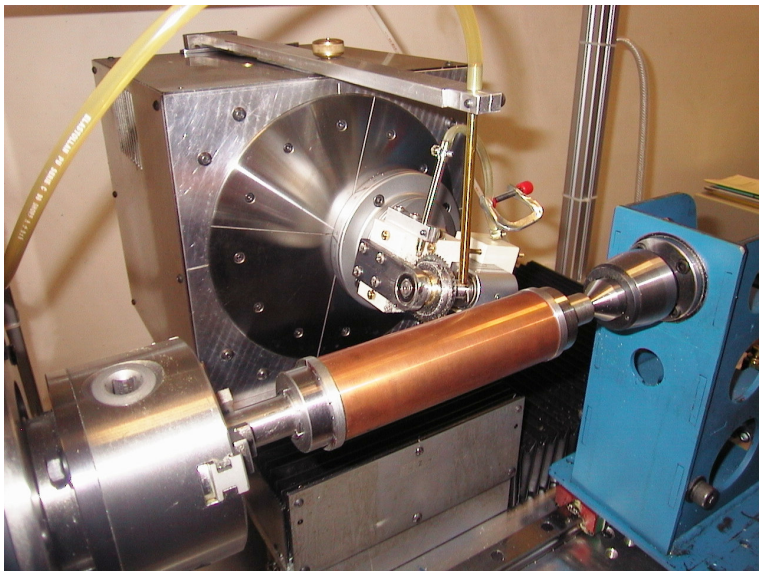

Fig. 6. **The magnet layer cutting system**

The specifications of the cutting system are such as to give the designer a complete freedom in defining the magnet geometry. The only restriction (if it can be considered as such) is that the cut thickness can not be smaller of 0.16 mm. This defines the minimum thickness of isolation between adjacent layers which, in order to minimize the packing factor in Eq.(2), should be as small as possible.

Table II lists the initial electrical and mechanical constraints used to calculate the magnet. The values were chosen on the basis of not only the target parameters of the magnet but also all the considerations mentioned above.

Published in **Advances in Inorganic Chemistry**, Vol. **57**, *Relaxometry of water-metal ion interactions*, Editors Rudi van Eldik R. and Ivano Bertini, Elsevier 2004 (ISBN 0-120-23657-5), pp.405-470.
This draft need not correspond to the final text. Reproduction is permitted for personal use only.

Table II. Starting electrical and mechanical constraints

Electrical		Mechanical	
B_{max}	1 Tesla	Number of layers	4
Max. available power	12-14 kW	Magnet length	100 mm
Max. power density	1.5 W/mm^2	Isolation thickness	0.16 mm
Metal resistivity	1.55x10^{-8} Ω.m	Internal radius (layer 1)	11.8 mm

After having subjected these starting data to the above described algorithm and optimized the values of B and dB/dt, one obtains the results listed in Table III.

Tab III. Parameters of the calculated magnet

B_{max}	1.143 T	Inductance	330 μH
V_{max}	30.1 V	Number of layers	4
I_{max}	400 A	Magnet volume	220 cm^3
Max.power density	1.1 W/mm^2	Internal bore	23.6 mm
Resistance	0.0747 Ω	Magnet length	100 mm

Apart from the calculated magnet parameters, the optimization software generates also a complete data set for cutting each of the four layers. Using these, one produces the real layers shown in Figure 7.

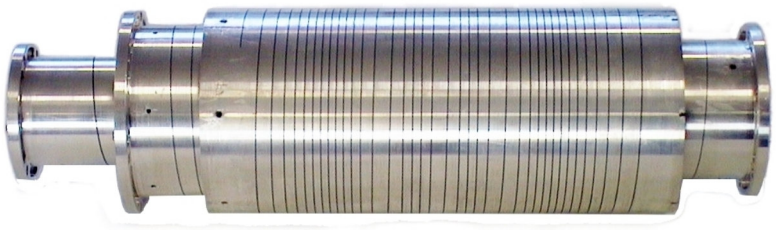

Fig. 7. **The four silver layers of a 1T FFC magnet.**

The pictures show also a detail of the inner wall of the smallest, most internal layer. The thickness of the cuts is 0.16 mm. At 400 A, the hottest spot power density dissipation reaches 1.1 W/mm^2. One of the most difficult engineering challenges is to cool these hot spots of the innermost layer efficiently enough to extract all the heat. If the cooling is inefficient, the layer can be seriously damaged or even destroyed.

Published in **Advances in Inorganic Chemistry**, Vol. **57**, *Relaxometry of water-metal ion interactions*, Editors Rudi van Eldik R. and Ivano Bertini, Elsevier 2004 (ISBN 0-120-23657-5), pp.405-470.
This draft need not correspond to the final text. Reproduction is permitted for personal use only.

Fig. 8. **The 1T magnet assembled inside its enclosure.**

Subsequently, the package of the four layers is mounted inside a special glass and Plexiglas container (Figure 8) which is designed to make the assembly mechanically rigid and, above all, to admit high throughput for the cooling liquid which it directs to flow flush with the surfaces of all the magnet layers.

The cooling of a magnet of the Noack-Schweikert type would not represent a problem if the power were dissipated uniformly on all its surfaces. What considerably complicates the task is the fact that the distribution is very non-uniform and, moreover, the highest power dissipation densities occur on loops with the smallest thickness and therefore the smallest surface area exposed to the cooling liquid (Figure 9). In addition, in order not to compromise the packing factor and thus the maximum achievable field, the gap between the layers must be kept as small as possible, leaving just the minimum clearance which can still guarantee a good cooling efficiency.

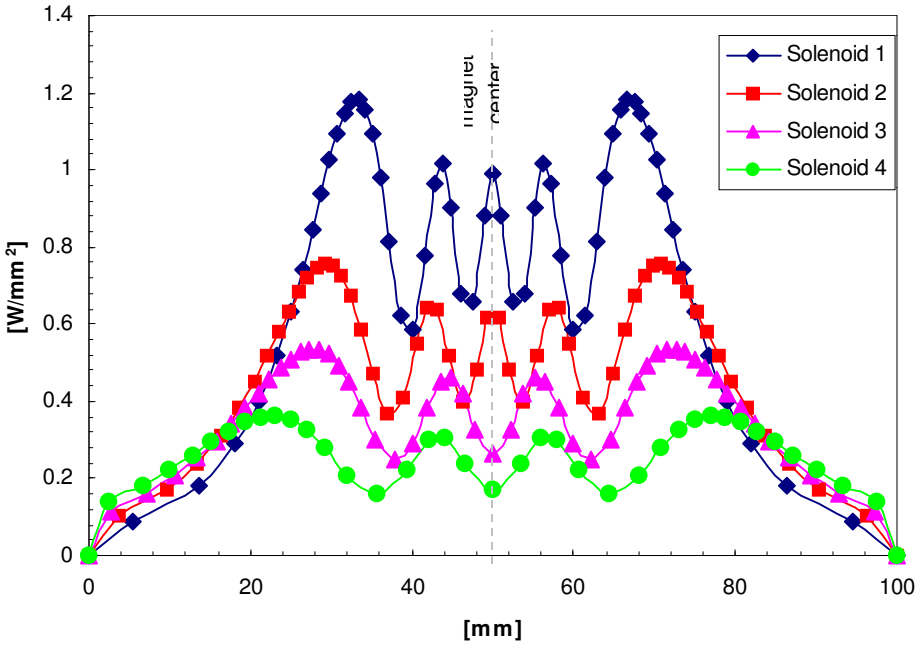

Fig. 9. **Distribution of power density along the four solenoids of the magnet.**

Published in **Advances in Inorganic Chemistry**, Vol. **57**, *Relaxometry of water-metal ion interactions*, Editors Rudi van Eldik R. and Ivano Bertini, Elsevier 2004 (ISBN 0-120-23657-5), pp.405-470.
This draft need not correspond to the final text. Reproduction is permitted for personal use only.

IV. Magnet power supply

IV.A. General considerations and peculiarities of an FFC power supply

Besides all the requirements dictated by any NMR application, a power supply designed to drive an FFC NMR electromagnet, whose peculiarities have been discussed in Section III. D, should satisfy a number of specific additional features.

The FFC magnet power supply should be designed as a *fast bipolar current source*. In order to match the low impedance of the magnet (fractions of Ohm), the output impedance of the power supply should be extremely low. We will see below that, in fact, the most convenient way to control the magnetic field B in an air-cored magnet is to control the current I flowing through the magnet to exploit the proportionality between B and I.

When designing a power supply for an FFC electromagnet system, one of the main challenges is to meet the extremely high field-switching slewing rates required in some FFC experiments, especially considering that the shortest measurable T_1 depends on the minimum switching time achievable by the magnet and the power supply combination.

From the electrical point of view, the theoretical minimum switching time is limited by the maximum power supply voltage and by the time constant L/R of the magnet with resistance R and inductance L. In a basic circuit like that shown in Figure 10 with a fixed power supply voltage V, when the switch trips on, the current evolves according to the equation

$$I(t) = \frac{V}{R}\left(1 - e^{-\frac{R}{L}t}\right). \qquad (5)$$

and the corresponding magnetic field B(t) increases proportionally to I(t).

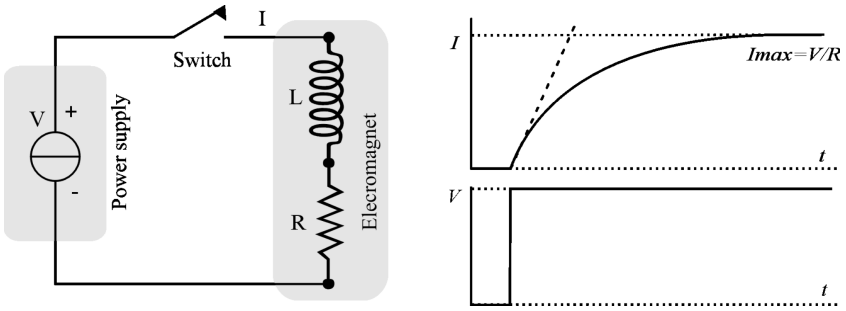

Fig. 10. **Evolution of the current in a switched R, L circuit**

When the switch is turned On, the voltage (bottom right) across the magnet jumps from 0 to V, while the current (top right) evolves according to Eq.(5). The starting slope of the I(t) curve (the dotted line), corresponding to the maximum field-slewing rate, is given by $V/L = (R/L)I_{max}$.

It is evident that, for a given magnet, it is the maximum power supply *voltage* which determines the maximum field-slewing rates and switching times while, according to Eq (2), the maximum available *power* determines the maximum achievable field.

Published in **Advances in Inorganic Chemistry**, Vol. **57**, *Relaxometry of water-metal ion interactions*, Editors Rudi van Eldik R. and Ivano Bertini, Elsevier 2004 (ISBN 0-120-23657-5), pp.405-470.
This draft need not correspond to the final text. Reproduction is permitted for personal use only.

IV.B. Historic solutions and a modern approach

In 1954 Packard and Varian *(74)* realized the first simple electronic circuit for switching between two field levels defined by two values of current, defined by R_{off} and $R_{mag,}$ as shown in Figure 11.

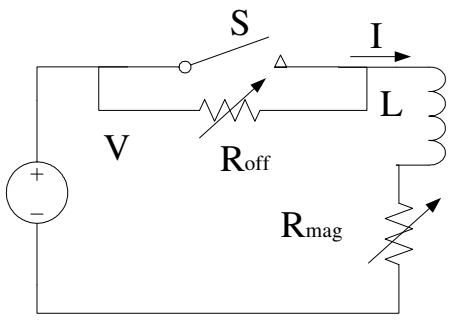

Fig. 11. **An early switching FFC circuit (Packard and Varian)**

The electronic switching methods used in the early days of the FFC technique look nowadays very simple. They were severely limited by the lack of suitable electronic power devices which would allow fast high-power switching on inductive loads. This problem was not limited to FFC and was eventually overcome by the development of modern power devices which allowed the introduction of switching methods with considerably better performance.

In 1968 A.Redfield et al. *(75)*, proposed an FFC power supply in which they introduced an energy storage circuit, whose specific purpose was to overcome the magnet inductance and reach the desired value of B in a shorter time while minimizing the required power. The most obvious method to rapidly switch the current in an inductive load without a substantial increase in the mean power consumption consists in applying a rather high voltage, but doing so only during the relatively brief switching intervals. Redfield's idea actually went a step beyond this simple principle. When a magnet is energized, there is a considerable amount of energy stored in its magnetic field. Upon switching off the magnet, this energy, rather then being wasted, can be used to charge a large storage capacitor to a high voltage. In a subsequent cycle, the energy stored in the capacitor is used to help energize the magnet by inserting the capacitor into the charging circuit and using it as a voltage booster. The result is faster field switching with only a marginal mean power increase.

In subsequent years, the above principle was used and further improved by Koenig and Brown *(58,66,78)*, Kimmich et al. (61,76,77) and Noack et al. *(65,75)*, leading to the realization of magnet/power supply systems with elevated slewing rates.

At present, modern power components such as GTO (Gated Transistor On/Off device), IGBT (Isolated Gate Bipolar Transistor), Power Mosfet (Metal Oxide Field Effect Transistor) and high voltage capacitors are easily commercially available and perfectly adequate to realize the energy storage switching system. Nevertheless, the realization of a complete power supply based on this method turns out to be costly and problematic when high reliability and routine usage are required. For this reason, starting in late 90's, Stelar introduced still another approach to the problem which is equally efficient but easier to implement. This approach, whose characteristics shall be discussed in detail the next two Sections, consists of:

Published in **Advances in Inorganic Chemistry**, Vol. **57**, *Relaxometry of water-metal ion interactions*, Editors Rudi van Eldik R. and Ivano Bertini, Elsevier 2004 (ISBN 0-120-23657-5), pp.405-470.
This draft need not correspond to the final text. Reproduction is permitted for personal use only.

i) controlling the magnet current rather than voltage and
ii) during the switching interval, making the current to vary along suitable and well defined waveforms.

The field-switching therefore becomes a rigidly controlled process rather than an on-off action, thus permitting to minimize field-switching times without having to use excessively high power-supply voltages and powers. The goal is to make sure that the system operates always in the linear region without hitting saturation conditions. The saturation of the power supply occurs when the sum of the induced voltage L(dI/dt) across the magnet terminals and the ohmic voltage RI exceeds the maximum available power supply voltage. In such a case, the power supply control loop exits from the linear region and is no longer capable of operating as desired.

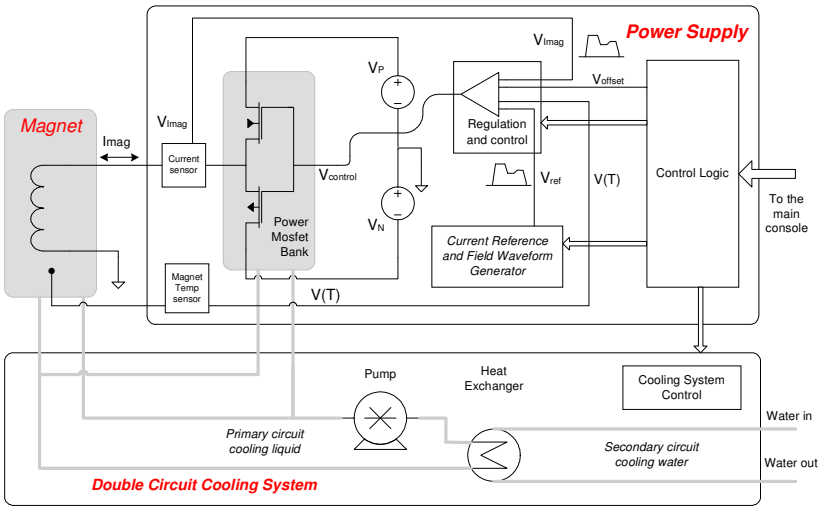

Fig. 12. **Block diagram of an FFC magnet power supply.**

Interconnections with the magnet and the cooling system are also shown.
For further details, see the text.

The functional block diagram of an FFC power supply based on these principles is shown in Figure 12. The *Current Sensor* generates a signal V_{Imag} which is proportional to the current I_{mag} flowing through the magnet. The *Regulation and Control* unit generates a control signal $V_{control}$ for the Power Mosfet Bank which, acting as a 'variable resistance', guarantees that the actual current I_{mag} ends up to satisfy the condition $V_{ref} = V_{Imag}$ at the input of the control comparator. V_{ref} is a reference voltage whose time dependence is defined by the control software during the measurement sequence programming. As a final result, the control loop guarantees that, apart from a proportionality constant, the time dependence of the magnetic field B reproduces that of the reference voltage V_{ref}, provided that the desired field-switching waveforms never cause the system to touch the saturation region.

Published in **Advances in Inorganic Chemistry**, Vol. **57**, *Relaxometry of water-metal ion interactions*, Editors Rudi van Eldik R. and Ivano Bertini, Elsevier 2004 (ISBN 0-120-23657-5), pp.405-470.
This draft need not correspond to the final text. Reproduction is permitted for personal use only.

IV.C. Switching time considerations and limits

We have already anticipated that in a power supply of the type represented by Figure 12, the current I(t) and the field B(t) are linearly related to the reference voltage V_{ref} only when the device operates in the linear region, clear of saturation. The power supply hits the saturation when

$$L[dI(t)/dt] + RI(t) = V_P \qquad \text{while switching up and} \qquad (6)$$

$$L[dI(t)/dt] + RI(t) = V_N \qquad \text{while switching down.} \qquad (7)$$

As usual, L and R are the inductance and the resistance of the magnet, while V_P and V_N are the extreme positive and negative voltages available from the positive and negative sections of the power supply, respectively.

Equations (6) and (7) define the conditions which the current I(t) should satisfy in order to achieve the fastest possible transition between any two current values comprised between zero and the maximum admissible magnet current I_{max}. When Eqs (6)-(7) are satisfied, in fact, the power supply is exactly at the edge of saturation but does not exceed it.

During the switching periods, the maximum current-slewing rate dI(t)/dt and, consequently, also the maximum field-slewing rate dB(t)/dt, are limited. For the current-slewing rate, the bounds follow directly from Eqs (6) and (7):

$$dI(t)/dt = [V_P - RI(t)]/L \qquad \text{while switching up and} \qquad (8)$$

$$dI(t)/dt = [V_N - RI(t)]/L \qquad \text{while switching down.} \qquad (9)$$

These equations can be easily integrated, giving

$$I(t) = (V_P/R)\{1-\exp[-(R/L)t]\} \qquad (10)$$

when switching from 0 to I_{max} and

$$I(t) = I_{max} \exp[-(R/L)t]+(V_N/R)\{1- \exp[-(R/L)t]\} \qquad (11)$$

when switching from I_{max} to 0.

In order to achieve symmetry between the cases of switching-up and switching-down, one needs to impose the condition

$$-(V_N/R)= (V_P/R) - I_{max} \qquad (12)$$

under which Eq. (11) becomes

$$I(t) = (V_P/R) \exp[-(R/L).t] - [(V_P/R)-I_{max}] \qquad (13)$$

The resulting fastest-switching waveforms, given by Eqs. (10) and (13) and shown in Figure 13, allow us to characterize the magnet - power supply system from the point of view of switching rates and times. In particular, they lead to the following expression for the minimum switching-up time mSwt for a complete transition from 0 to I_{max}:

$$mSwt = -(L/R)\cdot\ln[(V_P - RI_{max})/V_P] \qquad (14)$$

Thanks to the symmetry condition of Eq.(12), mSwt is equal to the minimum switching-down time for the complete jump from I_{max} to 0.

Published in **Advances in Inorganic Chemistry**, Vol. **57**, *Relaxometry of water-metal ion interactions*, Editors Rudi van Eldik R. and Ivano Bertini, Elsevier 2004 (ISBN 0-120-23657-5), pp.405-470.
This draft need not correspond to the final text. Reproduction is permitted for personal use only.

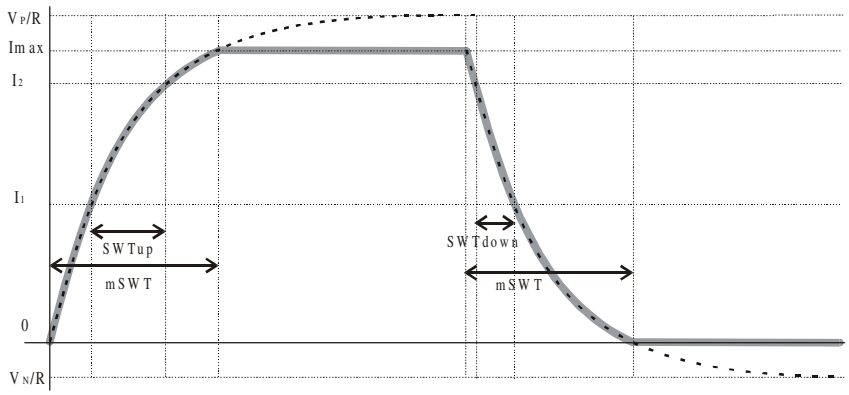

Fig. 13. **The fastest current-switching waveform**

The diagram shows the magnet current when switching between zero to the maximum admissible current I_{max}. The horizontal line at V_P/R corresponds to the maximum positive current which a power supply with voltage V_P can deliver into a magnet with resistance R. The line V_N/R defines the extreme negative current which can be generated by the negative power supply section with its extreme negative voltage V_N. The thick curve defines the fastest up- and down-going waveforms, clipped by the imposed limits of 0 and I_{max}. The two non-stationary sections have a generic exponential form with a time constant given by L/R, where L and R are the inductance and the resistance of the magnet. This defines the absolute minimum switching time mSwt and the fastest-approach waveform. If one wants to actively control the approach, it is necessary to take into account that, at any given current level **I**, the slope of the actual **I**(t) curve may not exceed that of the fastest-approach function.

More generally, one can ask what are the minimum switching-up and switching-dow times SWT_{up} and SWT_{down} for a transition between some arbitrary current levels I_1 and I_2 comprised between 0 and I_{max}. In this case, the resulting equations for the two times are slightly different:

$$SWT_{up} = (L/R).\ \{\ln[(V_P-RI_2)/(V_P-RI_1)]\} \qquad (15)$$

$$SWT_{down} = (L/R).\{\ln[(V_P+R(I_1-I_{max}))/(V_P+R(I_2-I_{max}))]\} \qquad (16)$$

Equations (15)-(16) express the shortest duration of the two switching intervals as a function of specific magnet and power supply parameters. The dependence of the SWT_{down} on V_N does not directly transpire from Eq. (16) but the importance of V_N in this context is evident from Eq.(12). We will discuss this point in more detail in the next Section.

IV.D. Why the bipolar configuration

As shown in the block diagram of Figure 12 and implicitly stressed by the discussion in the preceding Section, our power supply is of bipolar design, even though the magnitude of its maximum negative voltage $|V_N|$ is substantially smaller than that of its maximum positive voltage V_P.

This makes it possible to program - within limits - the sign of the magnet current and thus the orientation of the magnetic field B along the magnet axis.

Published in **Advances in Inorganic Chemistry**, Vol. **57**, *Relaxometry of water-metal ion interactions*, Editors Rudi van Eldik R. and Ivano Bertini, Elsevier 2004 (ISBN 0-120-23657-5), pp.405-470.
This draft need not correspond to the final text. Reproduction is permitted for personal use only.

In experiments at relaxation fields close to zero, the precision, resolution and stability of the absolute value of B_r become critical and a bipolar configuration, though it makes the design and implementation of the hardware more complex, improves the precision of the whole system and offers the following advantages:

- Reduced switching-down times, especially at low fields, as discussed in Section IV.C.
- Improved setting precision of the relaxation field for values close to zero
- Possibility to null the current offset due to electronic control components
- Possibility to null the axial component of the environmental magnetic field

In order to better illustrate these points, consider, for example, a magnet such as the one described in Section III.D. It reaches the maximum field of 1.143 T, corresponding to 48.7 MHz of ^{1}H Larmor frequency, with a current of 400 A. It follows that for a very low magnetic field corresponding to, let us say, 1kHz, one has to set a current of just 8 mA. In order to do that, one should be able to control the current with a precision and resolution of about 20 ppm of the maximum value! The required absolute precision is therefore of the same order of magnitude as the current offsets and thermal drifts of even the best analogue electronic components.

Precise null calibration of current offsets (which can be positive as well as negative) is possible thanks to the bipolar configuration of the power supply whose negative-going section has a much smaller range than the positive section and can be set with a considerably higher resolution. This increases the absolute precision of the field values for very small relaxation field settings and, in practice, makes it possible to extend the NMRD profiles to fields as low as a few tens of μT.

In a laboratory environment, a measured sample is subject not just to the field generated by the magnet but also - unless one implements particular screening or compensation devices - to all kinds of dispersed environmental magnetic fields due to, for example, the Earth magnetic field, electric power lines, other magnets, etc.

In a traditional magnet for NMR spectroscopy, the field B_0 of the magnet is much higher than the field components originating from outside sources. Moreover, devices such as efficient NMR field stabilizers are used to suppress all interfering external fields. Consequently, the presence of such field components can be usually ignored. On the contrary, during a FFC NMR measurement the sample may be subject to very low fields (ideally down to zero) which is practically impossible when the relaxation field value becomes comparable to the environmental fields. The amplitude of the such fields, if not compensated, represent therefore the lower relaxation field limit for a reliable NMRD profile.

Thanks to the bipolar configuration of the power supply, at least the static axial component ΔB_{env} of the environmental magnetic field can be easily compensated by means of a small current offset ΔI generating an axial field offset ΔB of the same value as $\Delta B_{env,}$ but of opposite sign.

For a complete suppression of the local magnetic field effects, however, one should compensate also its transversal component perpendicular to the magnet axis. This requires a pair of auxiliary coils, oriented in a correct direction in the magnet's azimuth plane, and capable of generating a transversal field component of the correct magnitude and sign (for more details, see reference (70).

Published in **Advances in Inorganic Chemistry**, Vol. **57**, *Relaxometry of water-metal ion interactions*, Editors Rudi van Eldik R. and Ivano Bertini, Elsevier 2004 (ISBN 0-120-23657-5), pp.405-470.
This draft need not correspond to the final text. Reproduction is permitted for personal use only.

IV. E. Power regulation banks

The power components used to drive the magnet current are an important part of the FFC power supply and can critically affect its performance. All together, these components constitute the power unit indicated in Figure 12 as the Power Mosfet Bank.

The power bank contains an adequate number (generally several tens) of linear solid-state power devices, such as transistors or power Mosfets. Because of the availability of modern power Mosfets that combine high performance with easy control, classical transistors are nowadays no longer used in applications of this type (in our case, we use channel-N and channel-P Mosfets for the positive and negative power supply sections, respectively).

In order to control the large required currents, all the power devices are electrically connected into a parallel array and, in order to dissipate the large amounts of heat generated during particular phases of the FFC experiments, the power array is actively cooled.

Figure 16 of next Section V shows the power dissipated by the magnet and by the power supply as a function of the magnet current. The total dissipated power, as well as its distribution between the magnet and the power supply, depend upon the working point which varies, often quite sharply, during an FFC cycle. The dissipated electric power is converted to heat which must be eliminated by means of a suitable cooling system. The power dissipated on a single Mosfet device can easily reach peak values of the order of 200-300 W, while the peak power dissipated by the magnet can be as high as 10-12 kW. This implies the use of an efficient cooling system employing, as we shall see later, a forced circulation of cooling liquid.

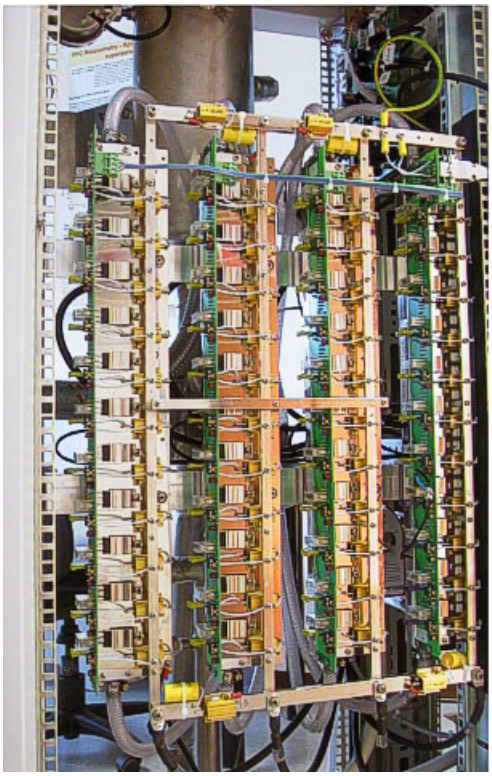

Fig. 14. **The power mosfet bank**

The positive section of the power banks shown in Figure 14 uses 40 type-N power Mosfet devices which can drive currents of up to 400 A. The same banks mount also 4 type-P devices for the negative section. The number of devices in the negative section is much smaller since the negative side is subject to much smaller power requirements. All 44 devices are mounted, together with their electronic control boards, on four special liquid-cooled, copper heat sinks. These, thanks to the excellent thermal conductivity of copper, combined with a design which maximizes the contact area between the copper and the cooling liquid, makes it possible to reach the requested cooling efficiency.

From the electric point of view, each Mosfet device is equipped with its own driver circuit which, in a case of failure, disconnects it from the parallel array. This is very important since it permits the system to operate properly even when a few power components have burned out. It is also extremely useful since it incorporates a possibility to easily locate any of the broken components.

Published in **Advances in Inorganic Chemistry**, Vol. **57**, *Relaxometry of water-metal ion interactions*,
Editors Rudi van Eldik R. and Ivano Bertini, Elsevier 2004 (ISBN 0-120-23657-5), pp.405-470.
This draft need not correspond to the final text. Reproduction is permitted for personal use only.

IV.F. Active compensation of the temperature dependence of B

We have mentioned earlier that, as shown in Figure 15a, small but perceptible magnetic field variations occur when the magnet temperature changes.

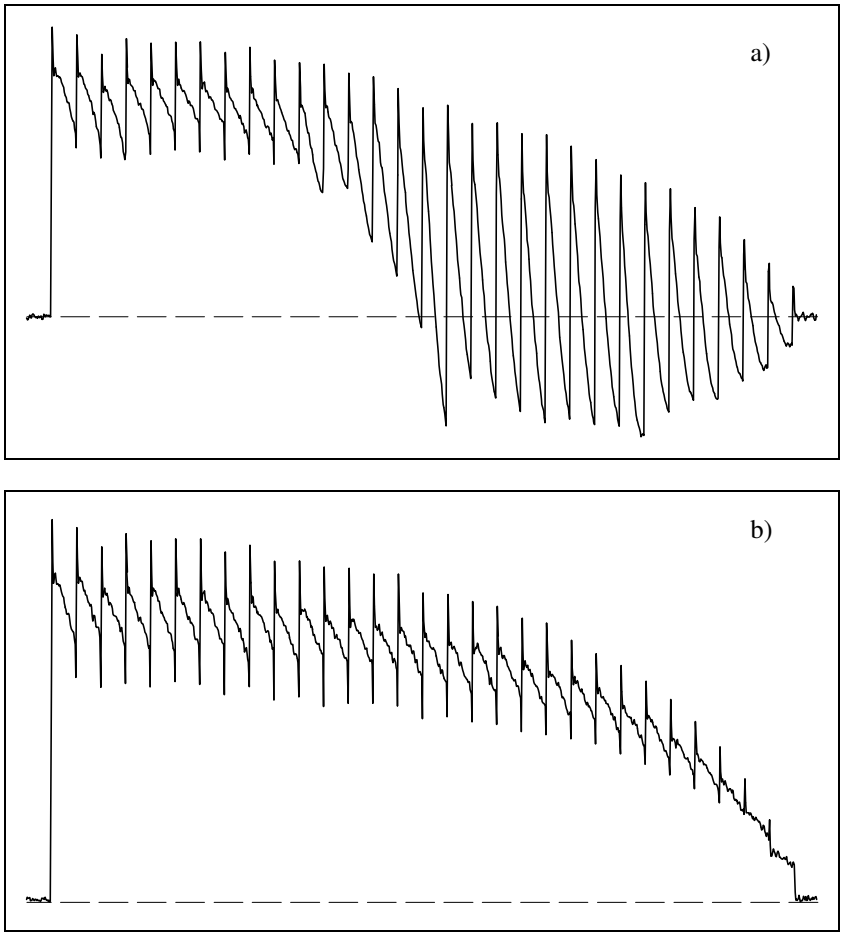

Fig. 15. **Data acquired in a multi-block NP experiment (32 τ-values).**

a) Experiment done with the thermal compensation turned Off. The FID offset is clearly not the same for all blocks, revealing magnetic field displacements due to magnet temperature fluctuations. The magnet temperature varies because the power dissipated on it in each block depends on the varying τ value.
b) The same experiment with the thermal compensation turned On.

The magnet temperature variation ΔT is approximately proportional to the power dissipated by the magnet and therefore to the square of the magnet current I. The variation of ΔB is a function of ΔT which reflects the changes in magnet geometry due to thermal dilatations. The net result is not easy to determine since it depends on many factors such as the magnet's geometry and its mechanical rigidity, the thermal properties of the used materials, the efficiency of the cooling system, etc. In practice, it is best to consider the ΔB(ΔT) dependence as an empirical characteristic of the particular magnet.

The knowledge of the relation ΔB(ΔT), combined with the actual magnet temperature T_{mag}, makes it possible to correct, at least in part, the magnetic field variations due to the varying

Published in **Advances in Inorganic Chemistry**, Vol. **57**, *Relaxometry of water-metal ion interactions*, Editors Rudi van Eldik R. and Ivano Bertini, Elsevier 2004 (ISBN 0-120-23657-5), pp.405-470.
This draft need not correspond to the final text. Reproduction is permitted for personal use only.

magnet temperature. The magnet temperature sensor shown in Figure 12 is used primarily for this purpose. Its output, after a transformation based on the empirical knowledge of the function $\Delta B(\Delta T)$ and on the known B(I) dependence, is fed-back to the control circuit of the power supply. Eventually, it generates a magnetic field variation equal to $\Delta B(\Delta T)$ but of opposite sign and thus compensates the original field-drift effect.

V. Cooling system

The cooling of the magnet and of its power supply constitutes in practice one of the major design challenges of an FFC relaxometer. The fact that one uses a resistive magnet and a power supply operating in the linear region implies a large power dissipation in at least some operating situations (Figure 16). The generated heat must be removed from the system by means of a suitable cooling system, like the one shown in Figure 17.

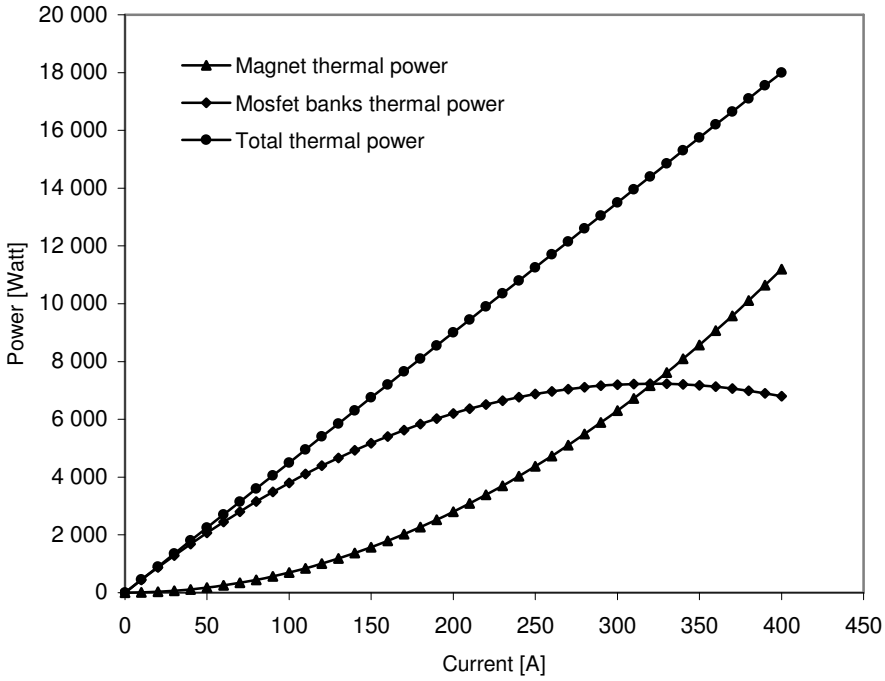

Fig. 16. **Distribution of dissipated electrical power between the magnet and the Power Mosfet bank**

As anticipated in Figure 12, the cooling system contains two thermally interconnected circuits.

The primary circuit is closed and filled with a special cooling fluid which, driven by a high-capacity pump, cools the magnet and the Power Mosfet banks. The cooling fluid is a commercially available product (Galden™) whose physical characteristics had been optimized for cooling electric devices wherever it is not possible to use water. It is chemically almost inert, absolutely non-toxic, and electrically non-conductive.

At first sight, it might appear preferable to use water as a cooling fluid since it has better thermal properties and lower viscosity. In practice, however, water had to be ruled out because of troublesome water electrolysis phenomena which can occur between windings of the solenoids when a voltage is applied accros the magnet..

Published in **Advances in Inorganic Chemistry**, Vol. **57**, *Relaxometry of water-metal ion interactions*, Editors Rudi van Eldik R. and Ivano Bertini, Elsevier 2004 (ISBN 0-120-23657-5), pp.405-470.
This draft need not correspond to the final text. Reproduction is permitted for personal use only.

The secondary circuit uses water from any water distribution network or, when possible, from a centralized cooled-water system. The heat dissipated from the magnet and from the power supply into the primary cooling circuit is transferred to the secondary circuit by means of a high-performance counter-current heat exchanger.

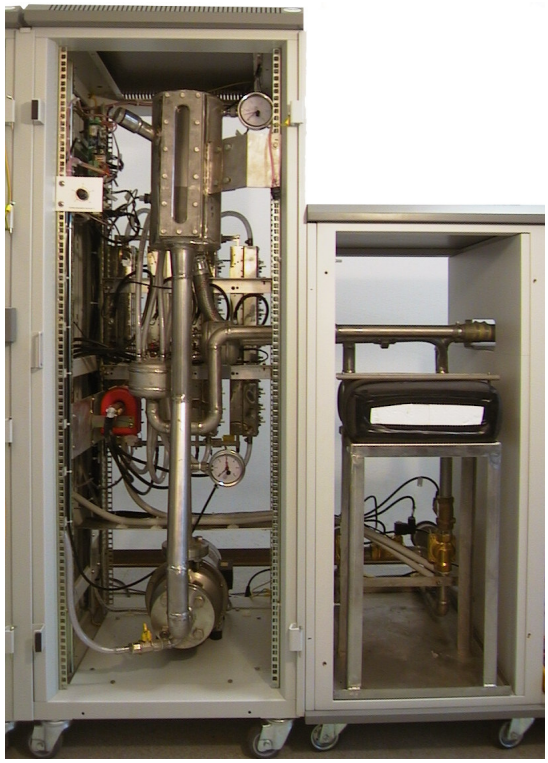

Fig. 17. **Cooling system of a 1 Tesla FFC NMR relaxometer**

VI. Signal detection probe

As far as technological principles are concerned, an FFC NMR detection probe does not differ from the probes of any other NMR instrument. Nevertheless, there are a few design characteristics of an FFC probe which are dictated by the type of the magnet used and its geometrical constraints.

Considering that, sensitivity permitting, one would like to measure NMRD profiles of any nuclide. The RF frequencies used on an instrument with a 1 T magnet like the one described in Section III.D range from about 3 MHz to over 40 MHz. One can hardly achieve a complete and efficient coverage of such a wide range with a single probe. In general, two or more tunable, broad-band probes are needed in order to be able to cover nuclides with low γ ratios such as deuterium, as well as high γ nuclides such as protons.

Considering the axial geometry of the FFC magnets, a number of practical problems makes it almost unavoidable to use a saddle-shaped detection coil with cylindrical Helmholtz geometry, even though it is well known that such a configuration is less efficient than a plain solenoid. To some extent, the situation resembles the one encountered in NMR spectroscopy when using axial superconductive magnets. In our case, however, the problem is further exacerbated by the fact

Published in **Advances in Inorganic Chemistry**, Vol. **57**, *Relaxometry of water-metal ion interactions*, Editors Rudi van Eldik R. and Ivano Bertini, Elsevier 2004 (ISBN 0-120-23657-5), pp.405-470.
This draft need not correspond to the final text. Reproduction is permitted for personal use only.

that saddle coils are very difficult to optimize at the relatively low RF frequencies characteristic of FFC NMR relaxometry.

An alternative to a saddle coil would be a solenoid coil which, however, would have to be oriented perpendicularly to the magnet bore and thus to the physical axis of the probe assembly. Due to spatial constraints, such an arrangement complicates considerably sample insertion, especially when the sample temperature has to be controlled and the assembly has to include an enveloping dewar for temperature control of the sample .

Fig. 18. **A FFC signal detection probe**

In our final realization (Figure 18), the probes use the Helmholtz coil geometry, favoring ease of use and efficient sample temperature control over a wide range of temperature values. The tunable, broad-band probe is inserted into the magnet from below and fixed to the bottom part of the magnet assembly in a simple way reminiscent of most high-resolution NMR systems. Thanks to this design, it is possible to use standard 10 mm NMR sample tubes which are inserted comfortably from above without any need to manipulate the probe.

VII. Control console

By the term console we intend all the electronic functional blocks used in a traditional NMR spectrometer, excluding the field control. In particular, it includes the following sub-systems:

- RF generation and gating
- Transmitter RF power booster
- RF receiver (gated quadrature phase detector)
- Low frequency signal handling (filters, amplifiers)
- Timing devices, including a pulser/sequencer unit
- Analog-digital converters
- Local CPU and firmware for Host-independent data acquisition management
- Sample temperature controller (VTC)
- Hardware interfaces
- Host data system
- Software

Actually, a console to be used with an FFC NMR relaxometer does not differ much from any conventional general-purpose NMR console. With the exception of the relatively simple interfaces controlling the magnet power supply and thus the field, all other hardware units are

Published in **Advances in Inorganic Chemistry**, Vol. **57**, *Relaxometry of water-metal ion interactions*,
Editors Rudi van Eldik R. and Ivano Bertini, Elsevier 2004 (ISBN 0-120-23657-5), pp.405-470.
This draft need not correspond to the final text. Reproduction is permitted for personal use only.

much the same as in any sufficiently versatile NMR spectrometer or relaxometer (what does differ quite a lot, of course, is the application software).

For this reason, a detailed description of the console in this paper is superfluous, except for a brief list of those features which, in our opinion, any research-grade FFC console should possess in order to guarantee maximum versatility of NMR dispersion measurements.

First of all, all the RF units are broad-band and the console must be able to operate in the full range of frequencies compatible with the maximum magnet field B_{max}. The first advantage which follows from such a choice is the possibility to observe, under optimal conditions, not only protons but many other interesting nuclides with a smaller gyromagnetic ratio γ, such as ^{2}H, ^{31}P, ^{23}Na, ^{19}F, etc. In principle, a console operating at a fixed-frequency ω would permit the observation of all nuclides for which $\omega \leq \gamma B_{max}$. However, in order to be able to measure nuclides with low γ values, one would have to choose quite low ω and thus penalize heavily the achievable signal-to-noise ratio (S/N) for nuclides with high γ values.

In order to understand this, consider that in an FFC experiment the amplitudes of the acquired signals are approximately proportional to the signal acquisition field B_a. For example, in the case of the basic pre-polarized sequence (to be described in Section VIII.C.), one can show (65) that

- When the relaxation period τ is zero, then $S \approx B_p B_a$, where B_p and B_a are respectively the polarization field and the acquisition field
- When τ is much larger than T_1, $S \approx B_r B_a$, where B_r is the relaxation field.

While the first factor in these expressions varies, the proportionality with respect to the acquisition field is always present. In order to maximize S/N, it is therefore advantageous to use always the largest possible acquisition field B_a and make the acquisition frequency match the corresponding Larmor frequency γB_a of the measured nuclide. This, however, can be done only when using a broad-band console.

From the previous paragraph it is apparent that, ideally, one should keep $B_a = B_{max}$. This is certainly true for slow-relaxing samples where the field-switching periods practically do not affect the measurements. In fast relaxing samples, however, one has to take into account the deleterious effects of the switching intervals when using very large field jumps. This matter shall be discussed in detail in Sections IX.B. and IX.E. What is relevant at this point is only the fact that, in order to maximize the measurement precision, keeping $B_a = B_{max}$ is *not* the best choice for samples whose relaxation rates are comparable to the magnet switching time. It follows that in such cases, the versatility offered by a broad-band console comes again handy.

Another important console feature regards the receiver detection method. This topic will be discussed from another point of view and in more detail in Section X. It is useful to mention, however, that the *only* type of receiver which offers *complete* information about the detected RF signal consists in a dual-channel quadrature phase detector. All other detector types (diode, envelope, power, ...) provide only a *partial* description of the signal which may occasionally mask some instrumental artifacts and thus look inviting, but which can never really replace a complete quadrature detector. The signals acquired by a quadrature detector can be used to recover any conceivable signal feature, while this is not true for the signals generated by other types of detectors. In particular, the quadrature signals allows one to calculate the signal modulus and thus make data evaluation insensitive to frequency offsets and receiver phase settings while, at the same time, maintaining the possibility to estimate and automatically correct such parameters. A dual-channel quadrature phase detector is therefore a must.

Published in **Advances in Inorganic Chemistry**, Vol. **57**, *Relaxometry of water-metal ion interactions*, Editors Rudi van Eldik R. and Ivano Bertini, Elsevier 2004 (ISBN 0-120-23657-5), pp.405-470.
This draft need not correspond to the final text. Reproduction is permitted for personal use only.

Another important feature regarding the whole receiver chain (including the probe and the preamplifier) is the total dead time which must be kept as short as possible in order to allow measurements of NMRD profiles of solids with extremely fast decaying FIDs.

As mentioned above, the parts which truly distinguish an FFC console from the consoles of traditional NMR instruments are the hardware and software interfaces through which one controls the magnetic field. They must permit the operator to set the different requested field levels (Off, Polarization, Relaxation and Acquisition) but also to control the field switching from one level to another according to a precisely time sequence which, moreover, must be rigorously synchronized with the concurrent RF pulse sequence. In addition, it must be possible to control the magnet slewing rate during the switching interval and thus the optimal switching waveform according to the principles discussed in Section IV.C.

Finally, we should mention the sample temperature control. It is a direct consequence of all relaxation theories that, in any FFC NMRD application, sample temperature is just as important as the dispersion curves themselves. In a sense, the temperature activates molecular motions while the field, by determining the nuclides Larmor frequency, defines a frequency 'window' through which to observe them. There is no way how the two effects could be separated or even just considered independently of each other. A precise sample temperature controller usable in a large range of temperatures is therefore to be considered not an accessory but an essential part of a FFC relaxometer.

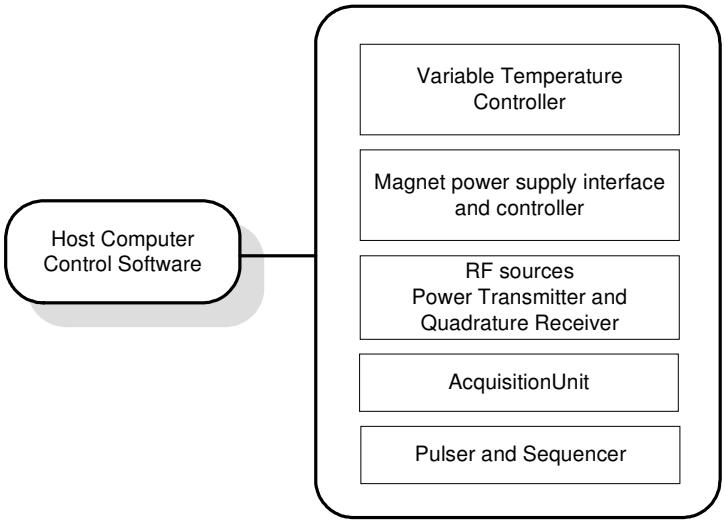

Fig. 19. **The main functional blocks of a NMR Fast Field Cycling Console**

Published in **Advances in Inorganic Chemistry**, Vol. **57**, *Relaxometry of water-metal ion interactions*,
Editors Rudi van Eldik R. and Ivano Bertini, Elsevier 2004 (ISBN 0-120-23657-5), pp.405-470.
This draft need not correspond to the final text. Reproduction is permitted for personal use only.

VIII. FFC data acquisition sequences

VIII.A. Special FFC features of elementary sequence intervals

Users of any NMR instrument are well aware of the extensive employment of what is known as *pulse sequences*. The roots of the term go back to the early days of pulsed NMR when multiple, precisely spaced RF excitation pulses had been invented (*17, 98-110*) and employed to overcome instrumental imperfections such as magnetic field inhomogeneity (*Hahn echo*) or receiver dead time (*solid echo*), monitor relaxation phenomena (*saturation-recovery*, *inversion recovery*, *CPMG*), excite and/or isolate specific components of NMR signals (*stimulated echo*, *quadrupole echo*), etc. Later on, employment of ever more complex pulse sequences of increasing complexity, combined with the so-called *phase-cycling* technique, has revolutionized FT-NMR spectroscopy, a field where hundreds of useful excitation and detection sequences (*111,112*) are at present routinely used to acquire qualitatively distinct 1D, 2D and 3D NMR spectra of chemical systems. A sSimilar evolution occurred also in the field of MRI (Magnetic Resonance Imaging) where specific pulse sequences (*113-116*) are used to enhance or modify the technique's spatial sensitivity and produce qualitatively distinct images of the investigated objects. It is therefore hardly surprising that pulse sequences play a crucial role also in FFC relaxometry.

Generation of precisely timed sequences of events requires the presence of a special device, known as the *pulser* (though *sequencer* would be a more fitting term). Considering that the development of new NMR techniques almost always involves new pulse sequences, research-grade instruments are necessarily equipped with general-purpose pulsers which, using a suitable software, can be programmed by the operator to generate *any* desired pulse sequence. The pulser mounted on Stelar FFC-Spinmasters, for example, features twelve output *channels* which can be be operated in a strictly synchronized manner to generate 12-channel control sequences of virtually any duration with absolute time resolution of 100 ns and a timing jitter inferior toless than 1 ns.

During the evolution of NMR techniques, the terms *RF pulse sequence* and *RF phase cycling* have undergone a considerable shift in meaning. Originally, they were used to indicate just the gating and phase-switching timing of the principal RF transmitter. In NMR spectroscopy, this has been soon complemented by the control of a second RF channel, the decoupler, leading to various *gated decoupling* sequences in which two physically distinct RF devices are operated in a synchronized manner. At present, pulse sequences often need to be synchronized also with devices other than the RF generators. Consider, for example, the UV flashes in CIDNP (Chemically Induced Dynamic Nuclear Polarization) investigations, field-gradient pulses in PFGSE (Pulsed Field-Gradient Spin Echo) self-diffusion experiments (*117*), homogeneity spoiling pulses (*106*) used in high-resolution relaxometry and, last but not least, the rigorously synchronized magnetic field gradient pulses which are an essential part of all MRI techniques (*113-116*).

One thus arrives at the concept of *pulser sequences* (rather than *RF pulse sequence*) in which the programmable pulser generates a *sequence of synchronized events* and controls a number of distinct devices. Analogously, the term *RF phase-cycling* is no longer appropriate (in Stelar terminology, it is replaced by *X-device cycling*).

In FFC relaxometry, the most conspicuous pulser-controlled device (apart from the RF excitation channel) is the magnet system. In other words, we generate B_0 field pulses of considerable amplitude, often switching the magnet field between zero and a maximum value of over 1T, and

Published in **Advances in Inorganic Chemistry**, Vol. **57**, *Relaxometry of water-metal ion interactions*, Editors Rudi van Eldik R. and Ivano Bertini, Elsevier 2004 (ISBN 0-120-23657-5), pp.405-470.
This draft need not correspond to the final text. Reproduction is permitted for personal use only.

we rigorously synchronize such B_0 pulses with the RF signal-excitation and/or preparation pulses. This, moreover, does not exclude the possibility to control other devices as well.

Like any sequence of events, an FFC experiment can be intended as a sequence of elementary intervals during each of which all system *control lines* maintain constant values. One needs to keep in mind, however, that while a control line transition is always very fast (settling times of the order of 1ns), the controlled device/parameter may require a much longer time to complete the requested state transition. In particular, for technical reasons explained in Section IV.C., the main magnetic field intensity can not change instantaneously and requires switching times of the order of a few ms.

In order to control the impact of the field-transient periods on the measured data, it is necessary to devise FFC sequences in such a way that each elementary interval falls into one of two possible categories:

- *fixed-field intervals*, in which B_0 is constant to within the desired NMR precision, and
- *switching intervals*, during which the field varies in a controlled way between a pre-programmed starting value and a pre-programmed final value.

In general, an FFC relaxation rate measurement requires a series of elementary experiments in which the duration τ of just one of the fixed-field intervals varies, while each of the switching intervals has always the same duration. Only in this way can one guarantee that the measured relaxation rate is correct and corresponds to the *relaxation field* present during the variable-duration interval (to be discussed later).

The performance of the field-switching circuitry (power supply and magnet dynamics) affects the minimum duration of the switching intervals. Figure 20 illustrates the principal characteristics of the field-switching waveform. Essentially, even though we talk about a single interval, it is composed of three physically distinct phases:

1) The *slewing phase* where the field is driven, following a linear ramp, from a starting value to a close vicinity of the desired final value. Following the argumentsation introduced in Section IV.C, one can show that, when a linear switching waveform is used, the maximum achievable slewing rate is given by

$$s_u \equiv dB/dt = (\kappa/L)V_p - (R/\kappa L)B = S_u - \alpha B \qquad (17)$$

when switching up ($s_u > 0$), and

$$s_d \equiv dB/dt = (\kappa/L)V_N - (R/\kappa L)B = S_d - \alpha B \qquad (18)$$

when switching down ($s_d < 0$).

Here κ is the proportionality constant between field and current ($B = \kappa I$), V_P and V_N are the maximum positive and maximum negative power supply voltage, L and R are the inductance and resistance of the magnet, B is the instantaneous main field value, $S_u = (\kappa/L)V_P$ and $S_d = (\kappa/L)V_N$ are the up-gowing and down-going slewing rates when $B = 0$, and $\alpha = R/\kappa L$.

Consequently, when switching from a field value B_a to a field value B_b, the minimum duration t_s of the linear switching ramp is

$$t_s = (B_b - B_a) / [S_u - \alpha B_b] \qquad (19)$$

when switching up, and

Published in **Advances in Inorganic Chemistry**, Vol. **57**, *Relaxometry of water-metal ion interactions*, Editors Rudi van Eldik R. and Ivano Bertini, Elsevier 2004 (ISBN 0-120-23657-5), pp.405-470.
This draft need not correspond to the final text. Reproduction is permitted for personal use only.

$$t_s = (B_b - B_a) / [S_d - \alpha B_b] \quad (20)$$

when switching down.

Using reasonably dimensioned power supplies, the minimum achievable t_s values are typically of the order of 1 ms.

Notice the presence of the field-dependent terms in the above formulae. They indicate, for example, that when the target field value is very large, the fastest up-going slowing rate drops down. Similarly, when the target field value is very low, it is the fastest down-going slowing rate to deteriorate. Among other things, this implies that when maximum system performance is required, the operator should keep in mind the dependence between the target field values to be used in the experiment and the maximum achievable slewing rates.

2) The *settling phase* where the field is already very close to its final value (with residual differences below 100 kHz of ^{1}H Larmor frequency) and settles down to its final value whose required reproducibility and stability is of the order of 100 Hz. Since the linearly driven ramp is no longer active, the dynamic characteristics of settling waveforms are different from those of switching waveforms. In general, there is a less conspicuous dependence on the field value (in some cases, the fine settling may actually take longer when the final field value is low). As far as the operator is concerned, it is usually sufficient if heto considers the settling phase as having an approximately constant duration.

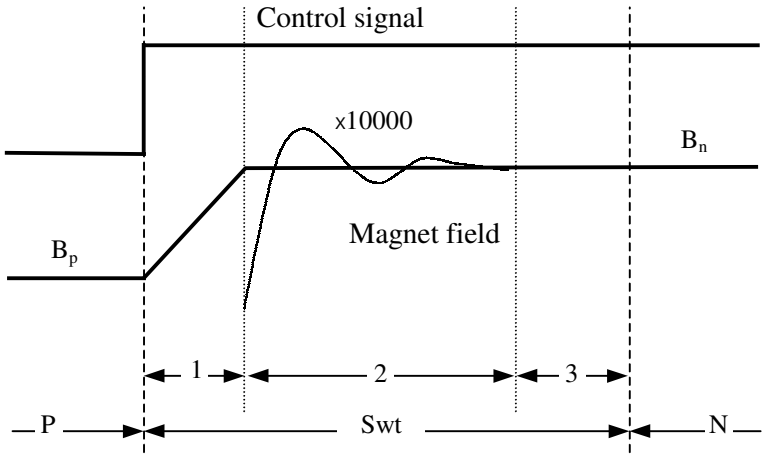

Fig. 20. **Schematic illustration of a main-field switching interval**

The single pulser interval Swt (switching time), nested between a previous interval P and a next interval N, is actually composed of three distinct phases (1,2,3). During phase (1) the magnetic field B is actively driven along a linear ramp from its previous value B_p to a close vicinity of its next value B_n. During the subsequent phase (2) it settles to its final value. The settling waveform is schematically represented by the thin line using a considerably expanded-scale. The switching margin phase (3) is a filler which simply completes the Swt interval. The operator controls the total duration of Swt and, within hardware-defined limits, the slope of the linear ramp but has no direct control of the settling waveform. He must make sure that the phases (1) and (2) fit within the Swt.

It is actually not always necessary to wait until the field has completely settled. There are only two situations where such a precision is really required:

Published in **Advances in Inorganic Chemistry**, Vol. **57**, *Relaxometry of water-metal ion interactions*, Editors Rudi van Eldik R. and Ivano Bertini, Elsevier 2004 (ISBN 0-120-23657-5), pp.405-470.
This draft need not correspond to the final text. Reproduction is permitted for personal use only.

a) When switching to the *acquisition field* at which the NMR signal shall be collected and
b) When switching to a low field value (below 100 kHz) where the settling waveform amplitudes represent an unacceptable field-setting error.

3) A *switching margin* which is treated as a part of the switching interval rather than a part of the subsequent fixed-field interval, even though the field is already stable. The usefulness of such switching margins stems from practical considerations. For example, they represent an important simplification for the operator. Since the duration of the switching margin does not affect the measured relaxation rates, the operator can often *uniform specify the same duration ofor all switching times* appearing in a pulser sequence, paying attention only to the requirement that the combined phases (1) and (2) must always fit within the switching time setting. The fact that such an approach leads, for some of the switching intervals, to somewhat excessive switching margins is often of little importance. Counter-indications to this approach regard only very fast relaxing samples where even a very small switching margin affects the precision of the measurements (we shall return to this point later).

VIII.B. Basic structure of any FFC sequence

Since all FFC experiments (except from a few set-up and/or diagnostic sequences) are a special variety of relaxation measurements, they are necessarily composed of three chronologically ordered sections or sub-sequences:

1. Preparatory sectionsub-sequence, during which the sample is subject to a sequence of field and/or RF pulses inducing therein a specific nuclear magnetization M_0. In general, M_0 can be characterized as a zero-quantum coherence state which, in most cases means simple I_z magnetization aligned along the direction of the main magnetic field. In some types of experiments, the starting M_0 state may may be simply null a zero magnetization.

2. Relaxation sub-sequencesection, during which the sample is kept for a time τ at a constant *relaxation field* B_r. The magnetization then evolves towards an equilibrium value $M(B_r)$, following a relaxation evolution curve $M(B_r,\tau)$, such that $M(B_r,0) = M_0$ and $M(B_r,\infty) = M(B_r)$. The primary goal of an FFC relaxometer is the acquisition of the $M(B_r,\tau)$ curves for a number of B_r values spread over many orders of magnitudes.

3. Detection sub-sequencesection, during which the sample magnetization is sampled by means of a more or less complex signal detection RF sequence. This occurs always at the signal *acquisition field* B_a determined by the current operating frequency (probe tuning etc) and the gyromagnetic ratio of the measured nucleus.

Using various detection sub-sequences, it is possible to select distinct nuclear magnetization components and thus discriminate between various sample components and/or distinct relaxation mechanisms. In combination with various possibilities of initial state preparation, this represents a powerful NMR relaxometry tool which, at present, is far from being completely exploited.

Published in **Advances in Inorganic Chemistry**, Vol. **57**, *Relaxometry of water-metal ion interactions*, Editors Rudi van Eldik R. and Ivano Bertini, Elsevier 2004 (ISBN 0-120-23657-5), pp.405-470.
This draft need not correspond to the final text. Reproduction is permitted for personal use only.

VIII.C. Elementary FFC sequences

As a starting example, let us now very briefly discuss the two simplest, text-book FFC experiments embodied in the PP (pre-polarized) and the NP (non-polarized) sequences.

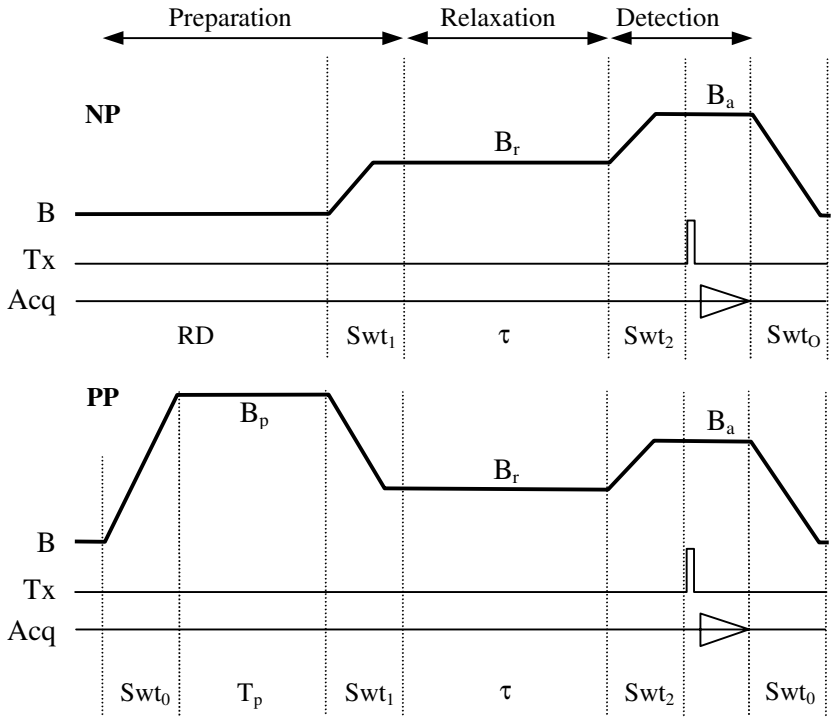

Fig. 21. **The basic non-polarized (NP) and pre-polarized (PP) sequences**

The thick line illustrates the behavior of the main magnetic field. The switching between the four preset field values (off, polarization B_p, relaxation B_r and acquisition B_a) is achieved by means of two control lines driven by the pulser. The pulser control lines for the RF transmitter gate (Tx) and data acquisition trigger (Acq) are also shown. Notice that from the end of the polarization sequence on, the two sequences are identical - what differs is only the sample magnetization at the beginning of the relaxation period. The various switching intervals Swt_i can be individually optimized, though this is rarely done. The start-up switching period Swt_0 and the final switching-off period Swt_O are normally not even programmed as explicit parts of the sequence (they have no effect on the acquired data) and the switching periods Swt_1 and Swt_2 are usually set equal to a common value Swt. The slopes of the linear switching ramps are all identical and their value can be preset by the operator prior to executing the sequence. For further details, see the text.

The **non-polarized sequence** (**NP**, Figure 21, top) is suitable for measurements of T_1 relaxation curves at relatively high relaxation fields (typically above a few MHz). The starting longitudinal magnetization M_0 is in this case null and is prepared by letting the sample relax in a null field for a time RD (recycle delay) which starts the sequence. The magnet is then switched to the desired relaxation field B_r where, after the rigorously constant switching period SWT_1 is over, it is kept for a variable time τ during which the sample magnetization grows towards the equilibrium value M_r corresponding to B_r. The magnet is then switched again, this time to the acquisition field value B_a and, once the constant switching period SWT_2 is over, a 90^o RF pulse is applied and the resulting FID is acquired. Immediately afterwards, the field is switched off and the whole

Published in **Advances in Inorganic Chemistry**, Vol. **57**, *Relaxometry of water-metal ion interactions*, Editors Rudi van Eldik R. and Ivano Bertini, Elsevier 2004 (ISBN 0-120-23657-5), pp.405-470.
This draft need not correspond to the final text. Reproduction is permitted for personal use only.

sequence is repeated (notice that the duration of the last switching interval is completely irrelevant and it does not need to be explicitly programmed as a specific pulser interval).

The **pre-polarized sequence** (**PP**, Figure 21, bottom) is suitable for T_1 relaxation measurements at low fields, theoretically down to zero value (in the present context we may neglect the phenomena (*70*) which make life a bit complicated at very low fields). The starting nuclear magnetization M_0 is in this case prepared by applying a strong *polarization field* B_p for a sufficiently long *polarization time* T_p. The result is a strong magnetization M_0 aligned to the field B_p. The magnet is then switched to the desired relaxation field B_r where, after the constant switching period SWT_1 is over, it is kept for a variable time τ during which the magnetization decays from M_0 towards M_r. Actually, starting from the end of the preparatory *sub-sequence*section, the two sequences are perfectly identical so that we can skip the details of switching to the acquisition field (SWT_2) as well as the description of signal acquisition.

IX. Acquisition and evaluation of complete relaxation curves

IX.A. Arrayed T_1 measurements

The acquisition of a complete relaxation curve $\mathbf{M}(\tau)$ consists in repeating an elementary NP or PP experiment while stepping τ through an array of values distributed according to a pre-defined *strategy* (linear, logarithmic, multi-range, etc, depending upon sample relaxation characteristics). All other instrument and sequence settings are kept rigorously constant so that any observed signal variation is due exclusively to the varying τ.

As shown in Figure 22, the resulting procedure, referred to as a multi-block experiment, produces a two-dimensional data set, such as an array of FIDs (its exact nature depends upon the signal acquisition method). The data of each τ-block are then reduced to a single quantity, $S(\tau)$ which should be proportional either to the total sample magnetization $M_a(\tau)$ or to one of its components. Since the vertical scale of the relaxation curve is irrelevant, we can identify $S(\tau)$ with $M_a(\tau)$ at the moment of detection (usually just after the first excitation pulse).

Regardless of what sequence one is using, reproducibility requires that the starting magnetization M_0 must be rigorously the same for all the τ-blocks, unaffected by whatever happened before each block started. One way to guarantee this is by imposing the following conditions:

1) For the NP sequence, we need $M_0 = 0$ which means that we must keep

$$RD \geq f^*.T_{1max}(0), \tag{21}$$

where RD is the recycle delay between the individual τ-blocks where the field is off and $T_{1max}(0)$ is the relaxation time of the sample at zero field and f is a factor to be discussed.

2) For the PP sequence, we need $M_0 = M_p$ (equilibrium magnetization at the field B_p) so that we must keep

$$T_p \geq f^*.T_{1max}(B_p), \tag{22}$$

where T_p is the duration of the polarization interval during which the sample is held at the polarization field B_p. In the PP-type sequences, the recycle delay RD is almost totally irrelevant and can be kept at 0 (magnet heating permitting).

Published in **Advances in Inorganic Chemistry**, Vol. **57**, *Relaxometry of water-metal ion interactions*, Editors Rudi van Eldik R. and Ivano Bertini, Elsevier 2004 (ISBN 0-120-23657-5), pp.405-470.
This draft need not correspond to the final text. Reproduction is permitted for personal use only.

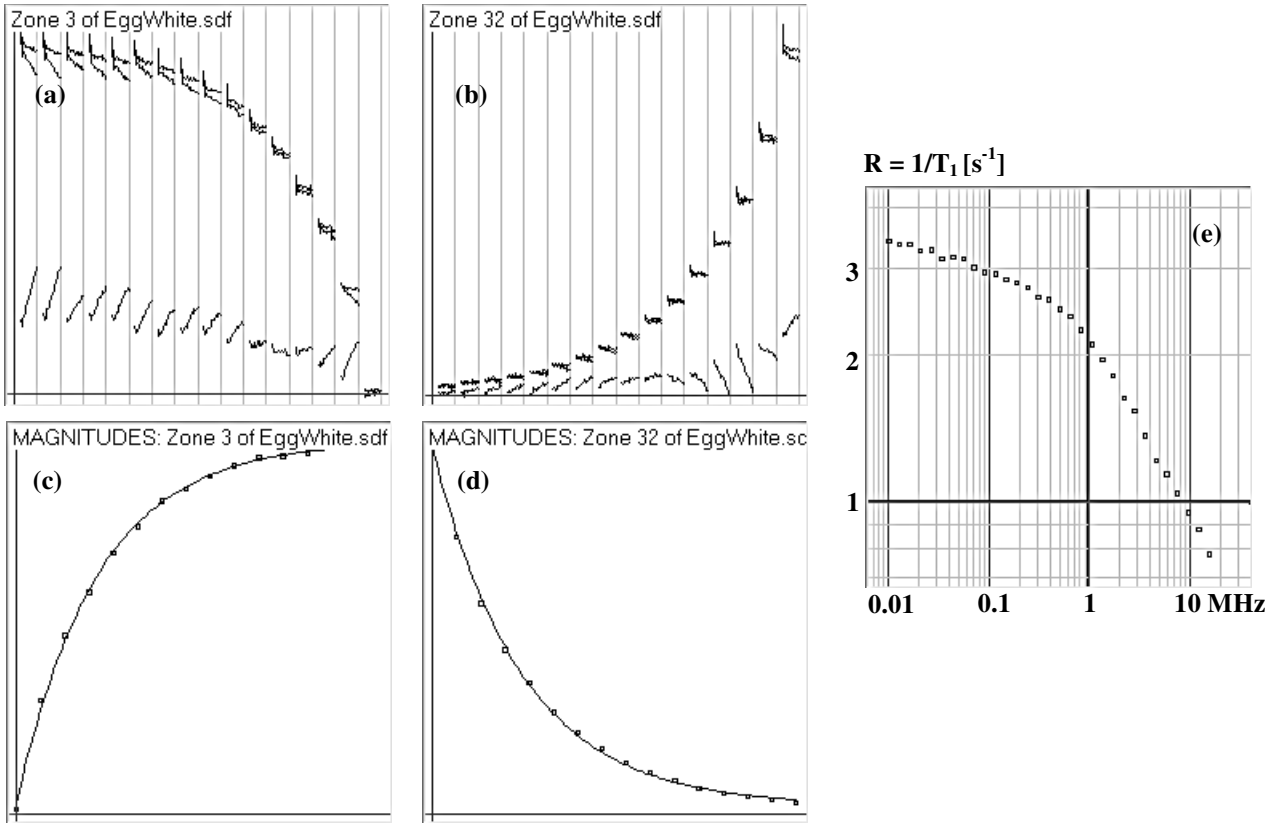

Fig. 22. **Example of various types of experimental FFC data**

The screenshots are shown exactly as they appear at the instrument. Graphs (a) and (b) show raw ^{1}H multi-block data (starting portions of FIDs), while (c) and (d) show the corresponding reduced data (1 point per block, obtained by averaging signal magnitudes over an FID window) and their mono-exponential fit. The data in (a) were obtained using the NP sequence and B_r =15 MHz, while those in (b) were obtained employing the PP sequence and B_r =10 kHz). To optimize magnet heating effects, the τ-values decrease from left to right. For each block, the real and imaginary components and the magnitudes of the signal are shown (originally colored). Graph (e) shows the whole profile in which every point corresponds to a complete multi-block experiment.

In both cases, f is a numeric factor and $T_{1max}(B)$ denotes the estimated relaxation time of the slowest-relaxing component of the sample magnetization in field B. One usually sets f = 4 which, assuming exponential curves, guarantees a relative precision of at least e^{-4} (about 1.8 %).

An important feature of the above equations is the fact that in the NP sequence we refer to relaxation times at zero field while in the PP sequence they are referred to the polarization field B_p. This does often make a big difference since, in many samples, $T_{1max}(0)$ may be much shorter than $T_{1max}(B_p)$.

Published in **Advances in Inorganic Chemistry**, Vol. **57**, *Relaxometry of water-metal ion interactions*, Editors Rudi van Eldik R. and Ivano Bertini, Elsevier 2004 (ISBN 0-120-23657-5), pp.405-470.
This draft need not correspond to the final text. Reproduction is permitted for personal use only.

Notice also that proper setting of the parameters RD and T_p requires an approximate knowledge of relaxation times, which are in their own term the objects of the investigation. This circular problemtautology makes it often necessary to carry out a few preliminary experiments before starting an actual relaxation curve acquisition. Fortunately, the values of RD and T_p do not need to be precise (a 20 % tolerance is quite reasonable) so that a simple recurrent estimation process converges to acceptable values in just one or two cycles.

IX.B. Effects of field-switching intervals

Though evaluation and interpretation of the relaxation curves does not directly regard the instrument, there is an instrumentation-related feature which affects evaluation and needs to be discussed.

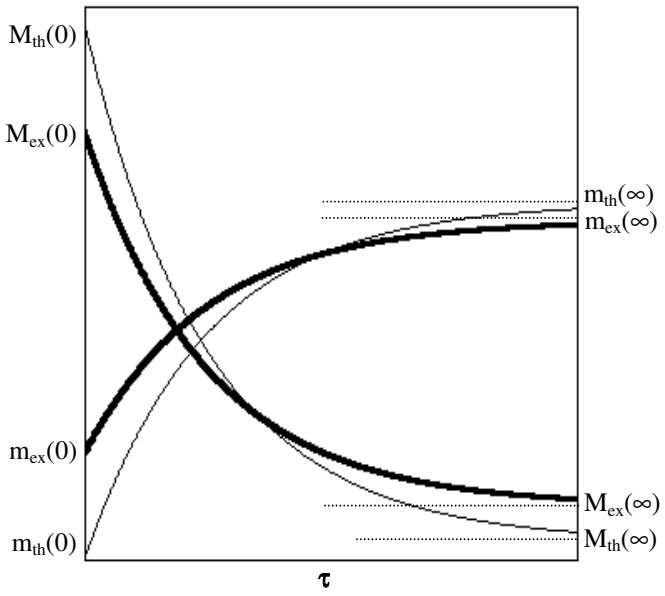

Fig. 23. **Effect of switching intervals on experimental M(τ) curves.**

The two theoretical (thin) and experimental (thick) lines represent two ad-hoc examples of the effect of switching intervals on the magnetization relaxation curves. In the case of an NP-type experiment (increasing curves with small-letter labels), the theoretical $m_{th}(\tau)$ function starts at $m_{th}(0) \equiv 0$ and increases toward the limit value of $m_{th}(\infty) \equiv m_r$, corresponding to the relaxation field b_r. The experimental curve $m_{ex}(\tau)$ starts at $m_{ex}(0)>0$ because of the first switching interval during which the field varies from zero to b_r. It then grows toward $m_{ex}(\infty) \neq m_r$ because of the second switching interval from b_r to the acquisition field B_a (in this example we assume $B_a<b_r$ so that the discrepancy has a negative sign). In the case of a PP-type experiment (decreasing curves with capital-letter labels), the theoretical $M_{th}(\tau)$ function starts at $M_{th}(0) \equiv M_p$ and decreases toward the limit value of $M_{th}(\infty) \equiv M_r$, corresponding to the relaxation field B_r (assumed here to be small but not-zero). The experimental curve $M_{ex}(\tau)$ starts at $M_{ex}(0)<M_p$ because of the first switching interval during which the field varies from B_p to B_r. It then falls toward $M_{ex}(\infty) > M_r$ because of the second switching interval from B_r to the (higher) acquisition field B_a.
Despite the apparent discrepancies due to relaxation during the switching intervals, the relaxation rate constants characterizing the evolution of the experimental curves with respect to τ are the same as those of the theoretical functions (all the curves plotted in this Figure have the same relaxation rate R).

Published in **Advances in Inorganic Chemistry**, Vol. **57**, *Relaxometry of water-metal ion interactions*, Editors Rudi van Eldik R. and Ivano Bertini, Elsevier 2004 (ISBN 0-120-23657-5), pp.405-470.
This draft need not correspond to the final text. Reproduction is permitted for personal use only.

One consequence of this situation is that the FFC relaxation curves can not be analyzed assuming any fixed starting or ending value. For example, under the mono-exponential hypothesis, the relaxation rate R (inverse of the relaxation time) must be estimated by fitting the three-parameter formula

$$M_{ex}(\tau) = c + w[1-\exp(-R\tau)], \qquad (23)$$

with no a-priori assumptions about the values of the constants $c = M_{ex}(0)$ and $w = M_{ex}(\infty) - M_{ex}(0)$.

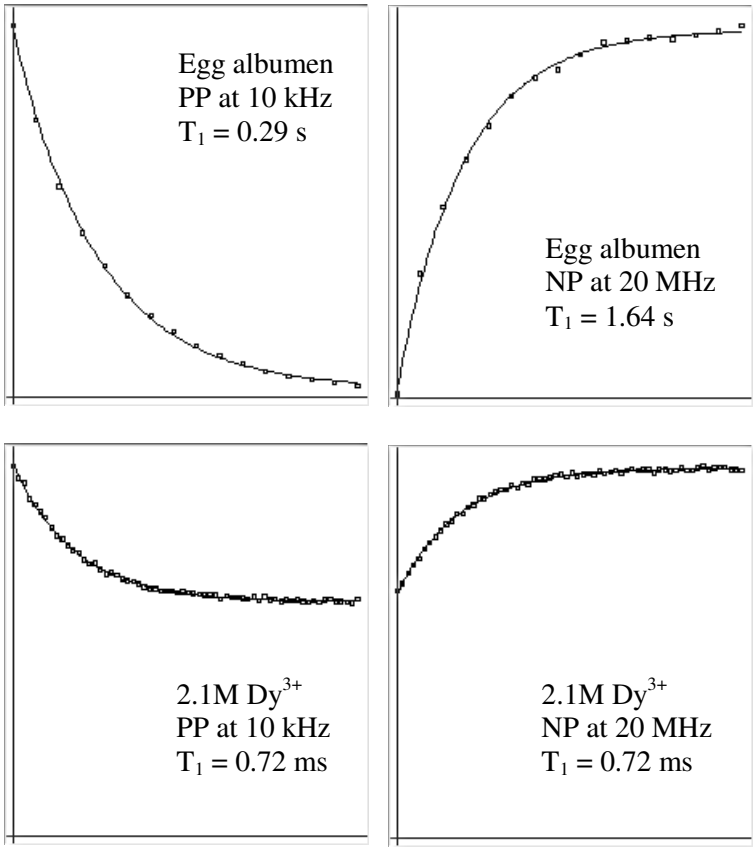

Fig. 24. **Examples of experimental relaxation curves**

The vertical scales are arbitrary, horizontal scales (τ-values) are linear. In all cases, the axes cross at the origin (0,0). The upper two plots regard a slow-relaxing sample in which the switching effects described in the text are negligible. The bottom two plots regard a very fast relaxing sample in which switching-interval effect are very pronounced.

The starting and final discrepancies between $M_{ex}(\tau)$ and $M_{th}(\tau)$ can be quite large (Figure 24 c,d). In fast relaxing samples, close to the high relaxation rate limit of an instrument, they may even exceed the total variation w of of the relaxation curve $M_{ex}(\tau)$. It is therefore necessary to ask whether the $M_{ex}(\tau)$ dependence on τ is still 'correct' in the sense that its generic type is still given by Eq. (23) with a relaxation rate R identical to that of the theoretical curve $M_{th}(\tau)$. Fortunately, the answer is affirmative (see Appendix A for a proof), provided that the field-switching waveforms are rigorously reproducible and independent of τ (no memory effects within the

Published in **Advances in Inorganic Chemistry**, Vol. **57**, *Relaxometry of water-metal ion interactions*, Editors Rudi van Eldik R. and Ivano Bertini, Elsevier 2004 (ISBN 0-120-23657-5), pp.405-470.
This draft need not correspond to the final text. Reproduction is permitted for personal use only.

magnet control system). On the other hand, as far as the problem at hand is concerned, the waveforms do not need to conform to have any particular shape (such as a linear ramp or other).

The only consequences therefore consist in the need for an extra parameter (c) in the fit and in a reduced dynamic range of the decay curves.

IX.C. Data accumulation methods

Like always in NMR (*118*), when the single-scan signal-to-noise ratio (S/N) is insufficient for a precise evaluation of the acquired data, it can be enhanced by averaging or, more frequently, accumulating, of data sets obtained in a number of repeated scans. Multiple-scan data accumulation opens also a number of novel experimental possibilities extending beyond the original goal of S/N ratio enhancement. Adding a bit of extra sophistication, in fact, data accumulation can be used to do any of the following:

a) Enhance S/N ratio,
b) Suppress the effect of a number of instrumental imperfections, and
c) Isolate particular components of the NMR signal.

The S/N ratio increases with the square-root of the number of scans, provided that the NMR signals are perfectly reproducible (except for the receiver noise). In FFC, this is not always true due to the main field instabilities, which often exceed the natural resonance line-width of the sample. In such cases, the rule applies well to the starting portion of the FIDs but not necessarily to the FIDs as a whole. This is one of the reasons why any free-evolution signals are rarely acquired for times longer than about 100 μs, even if the studied system would allow it. In order to extend this interval, one must resort to driven driven-evolution signal detection methods, such as the CPMG sequence with its spin-locking properties (to be discussed later).

Suppression of instrumental imperfections and/or selection of particular signal components are both based on the technique of phase cycling which exploits the dependence of NMR signals to on the variations of the RF phases of the transmitter pulse(s). S (since phase-cycling is used in every branch of NMR, we assume that the reader is acquainted with the technique) (we will provide later, while discussing signal detection methods). At this point we just wish to point out that phase-cycling is extensively used also in FFC and has to be supported by the console hardware - a requirement which implies pulser control of RF phases.

In practice, a particular 'phase cycle' is defined by means of an array of RF pulse settings (to be used cyclically during consecutive scans) and an associated array of 'receiver phases'. The 'receiver phase', however, does not correspond to any hardware device setting. Rather, it is an inter-locution for the various modes of how each single-scan signal should be handled by the data accumulation procedure (add, subtract, quad add, quad subtract, etc.).

In multi-block experiments we are stepping through the values of the arrayed parameter (such as τ). If, in addition, we also want to accumulate N scans, the following alternative arises:

a) Select the first arrayed-parameter value and carry out an N-scans accumulation (with phase-cycling). Then select the next arrayed-parameter value and repeat the whole process, stopping after all the arrayed-parameter values had have been handled.

b) Select the first phase-cycle settings and carry out a single elementary experiment for each arrayed-parameter value, storing the data in a global multi-block accumulation buffer. Then

Published in **Advances in Inorganic Chemistry**, Vol. **57**, *Relaxometry of water-metal ion interactions*, Editors Rudi van Eldik R. and Ivano Bertini, Elsevier 2004 (ISBN 0-120-23657-5), pp.405-470.
This draft need not correspond to the final text. Reproduction is permitted for personal use only.

select the next phase-cycle settings and repeat the passage, terminating after N such complete passages had have been completed.

We have here two possible cycles, one over the N scans with their nested phase-cycling, and the other one over the arrayed-parameter values. In the first case, the inner cycle is the one over the N scans, while in the second case, usually referred-to as *interleaving*, it is the one over the arrayed parameter values. Even though the two approaches are theoretically equivalent, the interleaved accumulation is preferred over the non-interleaved one. The reason is that, in a lengthy accumulation, any systematic long-term sample variations in the whole system (for example, sample deterioration) affect all the arrayed-parameter data blocks in approximately the same way. This is important, for example, when measuring samples subject to internal evolution on the time scale between several minutes and several days. Such systems are suprisingly common and include biological samples (for example, excised tissues) and materials subject to interesting internal-dynamics phenomena (phase transitions, polymerization, etc).

IX.D. Evaluation of the relaxation curves

There is are a number of ways by which how the data of an elementary FFC experiment (such as NP or PP) can be reduced to a single point of the $M_{ex}(\tau)$ curve. Since these data-reduction procedures depend upon the signal detection technique, we shall postpone their discussion. It is useful, however, to provide a few comments on how the $M_{ex}(\tau)$ curves should be evaluated once we have a set of experimental points $\{\tau_k,y_k\}$, where $y \approx M_{ex}(\tau)$ and $k = 1,2,...,n$, and n is the number of blocks in the multi-block experiment.

In the case of bi- or multi-exponential relaxation curves the treatment can be rather involvedquite complex (*119-123*). It becomes even more problematic Needles to say, the same is true forin systems with suspected continuous distributions of relaxation rates, where the whose evaluation numerical analysis of the decay curves(*124-128*) represents one of the mostan arduous mathematical problems (*124-128*). In general, evaluation tasks of this kind need to be treated off-line, using specific programs and algorithms.

However, a fast and simple mono-exponential on-line evaluation procedure included in the control software of an FFC relaxometer is not only possible but, in reality, is a must since it provides the operator with relaxation-rate data estimates essential for correct setting of acquisition parameters. The fact that the mono-exponential hypothesis may be inaccurate does not really change the fact that some kind of a preliminary estimate is essential for correct data acquisition.

In the following we review the on-line mono-exponential evaluation procedure we have chosen for on-line used on Stelar instruments. We believe that the qualitative features of this algorithm, such as the method used to estimate the probable error of the relaxation rate, represent a good example of how data should be handled also in more complex cases.

As explained above, under the mono-exponential hypothesis the data $\{\tau_k,y_k\}$ must be fitted by the three-parameter theoretical formula

$$y = c + w[1-\exp(-r\tau)], \qquad (24)$$

where c, w, and r are as yet unknown parameters. This requires a non-linear least-squares fit in which one minimizes the total quadratic deviation

Published in **Advances in Inorganic Chemistry**, Vol. **57**, *Relaxometry of water-metal ion interactions*, Editors Rudi van Eldik R. and Ivano Bertini, Elsevier 2004 (ISBN 0-120-23657-5), pp.405-470.
This draft need not correspond to the final text. Reproduction is permitted for personal use only.

$$Q(c,w,r) = \Sigma_k [y_k - \{c + w(1-\exp(-r\tau))\}]^2 \qquad (25)$$

with respect to c, w and r. It is convenient to split the task into two distinct parts.

1) Assuming the value of r to be fixed, Eq. (24) is linear with respect to c and w. The constrained optimal values of these two parameters, denoted as c_1 and w_1, are therefore easily determined using standard linear correlation formulae. Since c_1 and w_1 depend on r, this procedure defines the non-linear function $Q_1(r) = Q(c_1(r),w_1(r),r)$.

2) The minimum value of the function $Q_1(r)$ can be determined numerically using a standard algorithm such as Brendt interval bisection. Assuming that the minimum occurs at $r = r_2$, the value $Q_2 = Q_1(r_2) = Q(c_1(r_2),w_1(r_2),r_2)$ coincides with the absolute minimum of Q(c,w,r).

In addition to finding the optimal fit and thus the optimal relaxation rate $R = r_2$, this two-steps procedure provides us with the possibility to properly evaluate the *confidence interval* for R (Figure 25).

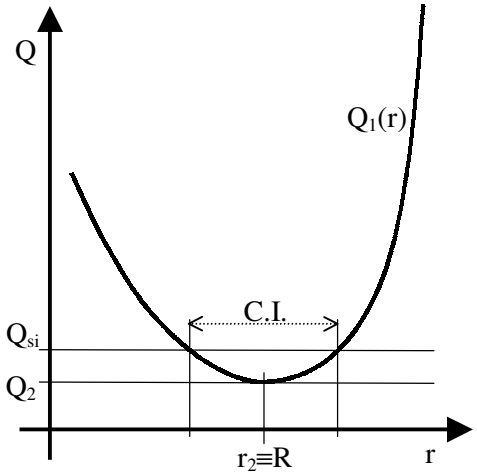

Fig. 25. **Determination of the R_1 confidence interval.**

$Q_1(r)$ is the total quadratic deviation assuming a relaxation rate value r and fitting all other parameters in Eq.(24). Its absolute minimum at r_2 defines the most probable relaxation rate R. Q_2 is the minimum of $Q_1(r)$ and Q_{si} equals Q_2 plus the least significant increment determined by statistical methods. This defines the confidence interval C.I. comprised between the two vertical lines. For more details, see the text.

We first notice that i) it is easy to evaluate the function $Q_1(r)$ for any r and ii) along the curve $Q_1(r) = Q(c_1(r),w_1(r),r)$, the parameters c and w vary so as to remain optimal for every value of r. The latter fact is essential since otherwise the confidence-interval estimates for r would be grossly over-optimistic. Numeric values of the *confidence interval* for R (regardless of the little interesting values of c and w) can be now be based on the least significant increment of $Q_1(r)$. Assuming that the optimum value Q_2 of the total quadratic deviation Q(c,w,r) is due entirely to random experimental errors, its least significant increment $\Delta_\alpha Q \equiv Q_{si}$ can be determined for any given significance level α by means of the *Fisher statistic* with both degrees of freedom set to (n-1). The confidence interval $\Delta_\alpha R$ for R then comprises all r values for which $Q_1(r) - Q_2 \leq Q_{si}$ and its *probable error* $e = (\Delta_\alpha R)/2$ is obtained, as usual, by setting $\alpha = 0.69...$ When, as expected, $Q_1(r)$ is approximately quadratic in the vicinity of the optimum, it turns out that the result can be

Published in **Advances in Inorganic Chemistry**, Vol. **57**, *Relaxometry of water-metal ion interactions*, Editors Rudi van Eldik R. and Ivano Bertini, Elsevier 2004 (ISBN 0-120-23657-5), pp.405-470.
This draft need not correspond to the final text. Reproduction is permitted for personal use only.

excellently approximated by the simple formula:

$$e = \sqrt{\frac{1}{(n-1)} \frac{Q_2}{Q_1''(r_2)}} \tag{26}$$

where $Q_1''(r)$ is the second derivative of $Q_1(r)$ which can be easily estimated by standard numeric methods.

When using the above algorithm as an on-line help, the operator must pay attention to the fact that, in general, the mono-exponential hypotheses need not hold. If, for example, the estimated fitting error is too large, the usual course of action would be to increase either the number of scans or the number of blocks. When, however, the apparent fitting errors are due to the fact that the relaxation curves are non-exponential, rather than to insufficient data quality, improving the precision of the $M_{ex}(\tau)$ curve is not going to help.

IX.E. Factors influencing the precision of relaxation rate estimates

Whatever is the fitting hypotheses and the corresponding evaluation algorithm, the evaluation results are burdened by experimental errors which depend primarily upon the following principal factors:

- Inherent signal-to-noise ratio $\rho = S/N$.
- Maximum relative magnetization $\mu = M_{max}/M_a$.
- Relative magnetization variation $\nu = (M_{max} - M_{min})/M_{max}$.
- Distribution and number n_b and of τ-values.
- Number of scans N.

A detailed discussion of the exact impact of each of these factors is beyond the scope of this paperChapter. Nevertheless, a few guidelines born out by experience are appropriate.

For a given number of nuclides placed in the sample coil volume, the inherent S/N ratio ρ is a parameter depending only on the probe and preamplifier assembly. It is usually measured in terms of the maximum FID amplitude after a 90^o pulse applied after the sample has reached its equilibrium magnetization M_a in the acquisition field B_a. Defined in this way, it is independent of the details of any FFC sequence.

The impact of ρ ratio on the relative precision of relaxation rate/time estimates is close to linear, meaning that doubling ρ reduces the relative errors by a factor of two.

The importance of the factor $\mu = M_{max}/M_a$ stems from the fact that in an actual FFC sequence, the maximum measured magnetization M_{max} is not M_a. For example, when switching-time effects are negligible, we have $\mu_{NP} = M_r/M_a = B_r/B_a$ for the basic NP sequence and $\mu_{PP} = M_p/M_a = B_p/B_a$ for the basic pre-polarized sequence.

The relative magnetization-variation factor $\nu = (M_{max} - M_{min})/M_{max}$ is related to the fact that if the magnetization did not vary with respect to τ, we could never determine R, no matter how large ρ and μ might be. The reason why we consider this factor independently of ρ is that, theoretically, it depends only on the pulser sequence type and, in pre-polarized sequences, on the ratio $\chi = M_r/M_p = B_r/B_p$. For example, one can easily verify that for the basic non-polarized and pre-

Published in **Advances in Inorganic Chemistry**, Vol. **57**, *Relaxometry of water-metal ion interactions*, Editors Rudi van Eldik R. and Ivano Bertini, Elsevier 2004 (ISBN 0-120-23657-5), pp.405-470.
This draft need not correspond to the final text. Reproduction is permitted for personal use only.

polarized sequences $\nu_{NP} = 1$ and $\nu_{PP} = (M_p - M_r)/M_p = 1 - \chi$, respectively, provided that switching effects are negligible.

Like in the case of the S/N ratio, the relative precision of relaxation rate/time estimates is linearly proportional to both the μ-factor as well as to the ν-factor.

The effect of switching times on the two factors can be inferred from Figure 23. For non-polarized sequences, we have $\nu_{NP} = [m_{ex}(\infty) - m_{ex}(0)]/m_{ex}(\infty)$ which is always smaller than the theoretical value of 1. This is also true for pre-polarized sequences, since it can be easily seen that the experimental value $\nu_{PP} = [M_{ex}(0) - M_{ex}(\infty)]/M_{ex}(0)$ is again smaller than the theoretical value.

The effect of switching intervals on ν-factor is therefore always a decrease in measurement precision - a problem which becomes dramatic in samples relaxing on a scale comparable to, or faster than, the switching times. In the case of the μ-factor, the switching interval effects are less dramatic and there is no universally valid rule, though a tendency toward degradation prevails (in any case, whenever there is a marginal enhancement of the μ-factor, it is always accompanied by a marked degradation of the ν-factor).

The type of the distribution of τ-values is a much -discussed topic. Experience shows that, in a mono-exponential case, the values should spread over an interval of more than $3*T_1$ but not much over $4*T_1$ T_1, and a linear distribution appears to be slightly better than a logarithmic one. This is probably due to the fact that in a three-parameter exponential fit, the points with large τ values play as crucial a role in determining the relaxation rate as the slope at small τ-values, and one needs both to determine R. On the other hand, it is evident that in multi-exponential cases, logarithmic distribution is often better suited for the task, especially when the relaxation rates of different sample components differ by an order of magnitude or more.

To describe the impact of the τ-values distribution type on the relative precision of relaxation rate estimates, we shall use a phenomenological factor f_d. We expect it to be independent of all the other factors, but dependent upon the type of relaxation rate quantity to be determined (for example, the fastest- or the slowest-relaxing component in a multi-component mixture).

For a given type of τ-values distribution, the size of the τ-values array (number of blocks n_b) plays approximately the same role as the number of scans N. Theoretically, the relative precision of any relaxation rate estimate is proportional to the square root of both n_b and N. This, of course, presumes that n_b is anyway large enough to carry out the analysis. For example, values as small as 4 may be sufficient in mono-exponential cases, while continuous distributions spreading over several orders of magnitude require a logarithmic distribution of τ-values and n_b values of over 100.

If we denote as ε the relative error of a particular relaxation rate estimate (or, for that matter, of any quantity related to relaxation-rates), the above discussion can be summed up by the following formula

$$\varepsilon^{-1} \approx \rho.\mu.\nu.f_d.\sqrt{n_b}.\sqrt{N} \qquad (27)$$

It is necessary to point out that the above discussion has been centered completely on the intrinsic experimental errors playing a role in the evaluation of a *single* relaxation curve. This is not the same as the *reproducibility* of the results (scatter) when the whole multi-block measurement is repeated. When comparing single-fit errors with the overall scatter, two situations arise:

Published in **Advances in Inorganic Chemistry**, Vol. **57**, *Relaxometry of water-metal ion interactions*, Editors Rudi van Eldik R. and Ivano Bertini, Elsevier 2004 (ISBN 0-120-23657-5), pp.405-470.
This draft need not correspond to the final text. Reproduction is permitted for personal use only.

a) In a mono-exponential case the scatter is typically about twice as large as the fitting errors and the two quantities are correlated.

The discrepancy is due to sources of errors not contemplated considered in the above expositiondiscussion, such as field noise and reproducibility, thermal effect etc. In particular, thermal effects on the magnet are important since experience shows that the scatter increases when the relaxation field and/or the polarization field are close to the upper limit of the magnet. Since all such contributions are random, prolonged data accumulation reduces both the fitting errors and the scatter.

b) When the mono-exponential hypotheses does not hold, the fitting error reflects the discrepancy between the hypotheses and the data, rather than any random characteristics of the experimental $M_{ex}(\tau)$ curve. Consequently, situations may arise when the fitting errors are much larger than the scatter. Prolonged data accumulation, in particular, reduces the scatter but, beyond a certain point, has little or no effect on the fitting errors.

IX.F. Optimization of relaxation rate measurements

When is an experiment, or a series of experiments, optimal? The answer to this often asked question (*129*) is not unambiguous because, as in most optimization problems, it involves multiple and mutually contradictory criteria, such as

- Minimum measurement time.
- Minimum scatter (best reproducibility) achievable in a given time.
- Capability to falsify/confirm specific application hypotheses.

Here, of course, we can only concentrate on the first two points. There is always the necessity to find a compromise between the maximum affordable measurement scatter and the data accumulation time necessary to reach it. To a considerable extent, the operator can influence the resolution outcome of this compromise by placing a premium either on the precision or on the speed which is achieved primarily by adjusting the number of blocks in the multi-block experiments and the total number of scans.

A little bit less obvious is the setting of the recycle delay RD (for NP-type sequences) or T_p (for PP-type sequences) which is linked through the factor f in Eqs. ([3)] and ([4)] to the estimated relaxation time T_{1max} of the slowest-decaying component of sample magnetization at a specific field. One cannot influence the sample relaxation times, of course. On the other hand, the relaxation times usually dominate the overall duration of a single multi-block scan so that, except for fast relaxing samples, substantial measurement-time savings can be achieved only by acting on the parameters linked to the relaxation.

All this points to the factor f, which guarantees that the sample magnetization at the beginning of each block is the same with a relative precision of e^{-f}. However, the actual reproducibility is much better than this, since we do not really need M_0 to be exactly zero (in NP) or M_p (in PP) but only that they be the same for all τ-blocks of a multi-block experiment. Theoretically, considering that the acquisition period of the previous block normally destroys the longitudinal magnetization and the subsequent sequence of events until the start of the next relaxation period is the same for every τ-block, any value of f should be theoretically acceptable. Further investigation of these aspects is currently under way.

Published in **Advances in Inorganic Chemistry**, Vol. **57**, *Relaxometry of water-metal ion interactions*, Editors Rudi van Eldik R. and Ivano Bertini, Elsevier 2004 (ISBN 0-120-23657-5), pp.405-470.
This draft need not correspond to the final text. Reproduction is permitted for personal use only.

In very fast relaxing samples ($R >> 10\ s^{-1}$), the contribution of the switching intervals to the total measurement time becomes appreciable and is therefore susceptible of possible optimization. The common practice is to set the duration of all switching intervals in a sequence to the same value Swt which has a safety margin to include the ramp phases as well as the settling phases of all switching periods (see Figure 20). This is quite fine for samples in which all relaxation times are consistently much longer than Swt. Otherwise, individual optimization of the switching times is advisable for two reasons:

- it reduces total measurement time (though this has usually a rather modest effect), and
- it enhances the relative magnetization variation $\nu = (M_{max} - M_{min})/M_{max}$ of the experimental $M_{ex}(\tau)$ curve and thus, through Eq. (27), directly affects the measurement precision, often in a marked way.

The optimization of individual switching intervals exploits two principles:

- Extremely precise field settling (well below 0.1 %) is required only when switching to the acquisition field where RF pulses are to be applied and/or the NMR signal is to be collected. In all other switching periods (for example, switching from the polarization field to the relaxation field), field-settling precision of the order of 0.1 % is quite sufficient.
- The duration of the ramp phase of a switching interval depends upon the field levels between which the switching actually occurs and can be therefore individually adjusted (see Eq. 2).

Before concluding this Section, we should mention another, more basic choice the operator (or the instrument's software) has to make, namely the selection of the type of sequence to be used. Whether one should use a non-polarized or a pre-polarized sequence depends essentially upon the relaxation field value B_r. The choice affects the precision of the measurements basically through the product of the factors μ and ν in Eq. (27). For the ideal NP and PP sequences, these products are $\mu_{NP}\nu_{NP} = (B_r/B_a)$ and $\mu_{PP}\nu_{PP} = (B_p/B_a)(1 - B_r/B_p)$ and it is elementary to see that $\mu_{NP}\nu_{NP} > \mu_{PP}\nu_{PP}$ when $B_r > B_p/2$ and vice versa. Theoretically, therefore, one should use the PP sequence for relaxation fields B_r smaller than half the polarization field value and the NP sequence for relaxation fields higher than that.

In practice, this is the best choice for all samples, except those which relax very fast and, in addition, relax much faster at low fields than at high fields (large overall dispersion). In such cases, the degradation of the ν-factor due to the effect of switching periods is substantially higher for the NP sequence (which starts always from zero field) than for the PP sequence (which never descents below B_r) and therefore the NP sequences should be disparaged by moving the B_r switchover level should be moved slightly above $B_p/2$ (typically 60-65 % of B_p). Again, exact formulae describing this kind of optimization are not yet available and further research is in progress.

X. Signal detection and analysis

In FFC relaxometry, one is concerned with the time evolution of the parallel component M of the nuclear magnetization of a sample or, in more complex cases, of one or more of its constituents. The primary scopegoal of the signal detection is to estimate M and not, like in NMR spectroscopy, to analyze the FIDs in any detail beyond a simple solid/liquid phase distinction.

Published in **Advances in Inorganic Chemistry**, Vol. **57**, *Relaxometry of water-metal ion interactions*,
Editors Rudi van Eldik R. and Ivano Bertini, Elsevier 2004 (ISBN 0-120-23657-5), pp.405-470.
This draft need not correspond to the final text. Reproduction is permitted for personal use only.

In principle, therefore, FFC relaxometry could employ - and often does so - a number of detector types such as phase detectors, diode detectors, square detectors, modulus detectors, envelope detectors, SQUID detectors, etc.

In any case, however, tThe NMR signal can be acquired only after $M_{\parallel}$ has been brought to the XY detection plane which, of course, is achieved by means of a suitable NMR excitation sequence. There is little conceptual difference between the FFC excitation sequences and those used in other NMR techniques. The NMR types of signals used in FFC include all the "classical" ones, such as free induction decays (FID), spin-echoes, envelopes of CPMG spin-echo trains, etc. In principale, any NMR signal is acceptable, as long as the acquired signal it reflects M at the end of the relaxation period. The Classical NMR signal excitation and preparation methods can be used also to select or/ enhance particular components of nuclear magnetization.

In general, the signal acquisition process provides us with more data than needed. To extract relaxation parameters, we need a single value $M(\tau)$ for each τ setting, but we generally acquire a whole array of values. Clearly, some kind of data-reduction process must be implemented before the acquired signals can be used in the way we intend. Like the NMR excitation techniques, the data reduction process can be exploited to enhance or suppress particular signal components.

This delimits three aspects of FFC signal detection (detector hardware, excitation & detection method, and data-reduction algorithm). The following paragraphs expound explain briefly the most popular ways choices we have made to handle these aspects.

X.A. Hardware detection

From the practical point of view, dual-channel phase detectors operated in quadrature appear to be the best hardware-detection choice. Unlike the other techniques mentioned above, phase detection is sensitive to the signal's to RF frequency offset from resonance and to the RF phase which, on the one hand, makes it more complex to use (as well as and more sensitive to instrument instabilities) but, on the other hand, it leads to a number of important advantages, such as:

- *Linearity*. Phase detection is truly linear, in the sense that a multi-component sample magnetization leads to a signal which is guaranteed to be a simple linear superposition of contributions from the individual components. All other detection methods lead to signals containing cross terms between different components as well as non-linear coupling cross terms between the signal and the noise.
- Applicability of standard NMR *phase-cycling* data accumulation methods.
- Precise *definition of receiver bandwidth* by means of audio filters (improves sensitivity).
- *Sensitivity enhancement* due to the fact that we are using two uncorrelated detectors.
- Improved *control of experimental conditions*. Phase detection prevents the operator from straying from resonance, makes possible reliable offset estimates and receiver phase estimates and even completely automated maintenance of optimal offset settings.
- Possibility of *complete spectral analysis* of the acquired signals. Though FFC is still a low-resolution technique, this is sometimes useful and it appears as an important potential advantage for future developments.

Modern instruments usually offer an on-board choice between a quadrature phase detector and some kind of diode or square detector. The latter, however is mostly used just for instrument

Published in **Advances in Inorganic Chemistry**, Vol. **57**, *Relaxometry of water-metal ion interactions*, Editors Rudi van Eldik R. and Ivano Bertini, Elsevier 2004 (ISBN 0-120-23657-5), pp.405-470.
This draft need not correspond to the final text. Reproduction is permitted for personal use only.

setup (probe tuning, etc) while signal acquisition is done almost exclusively by the phase detector.

As usual, we shall from now on consider the output of the dual-channel phase detector as a unique complex signal, with the outputs of the two channels identified with its Cartesian components.

X.B. Post-detection signal handling

By revealing all aspects of the signal, the phase detector brings to foremakes evident also all instrumental artifacts which would not be observable with another type of detection. On an FFC instrument, this typically includes thermal field drifts (see Section IV.D) and field instabilities associated with the large dynamic bandwidth of the switching magnet system.

In a certain sense, the detector provides us with more details than what we have bargained for. The goal of the primary post-detection signal handling is to get rid of those features which are irrelevant in a given context and enhancing those which are essential. In many cases, for example, it makes no sense to analyze the shape of an acquired FID, and the only desired quantity is the total amount of the signal (a single number rather then a dual data array).

There are various approaches to the data-reduction task. An often used one consists in of computing the modulus of the complex phase-detector signal. This removes all offset imperfections as well as any receiver phase misadjustment, bringing us theoretically to what we would have by summing the outputs of two independent, ideal diode detectors. In this case, however, the original signals are still available and can be used to check various aspects of data quality, carry out additional corrections (such as removal of noise-rectification artifacts) or submitted to alternative evaluation algorithms.

The modulus data are then used to estimate the total signal amount by means of various algorithms. The simplest one uses the average of the modulus over a pre-defined data-array window.

For evident reasons, this topic overlaps with the much broader field of application-specific data evaluation methods which we will occasionally mention but whose comprehensive exposition exceeds the scope of this paper.

X.C. NMR signal excitation &detection sequences

In this Section we shall list and briefly discuss the pros and cons of some classical NMR techniques used for signal excitation and acquisition.

1. Simple FIDs (Figure 22)

The simplest method of detecting longitudinal magnetization consists in applying a 90^{o} RF pulse and acquiring the resulting FID. Though at first sight this appears as the most obvious approach, it is not void of drawbacks.

One problem is the dead time of the probe-preamplifier subsystem (the combined effect of probe RF ringing and of preamplifier recovery from saturation). While irrelevant in samples with long enough FID (above 0.1 ms or so), it may become a major limitation with fast-decaying FIDs

Published in **Advances in Inorganic Chemistry**, Vol. **57**, *Relaxometry of water-metal ion interactions*, Editors Rudi van Eldik R. and Ivano Bertini, Elsevier 2004 (ISBN 0-120-23657-5), pp.405-470.
This draft need not correspond to the final text. Reproduction is permitted for personal use only.

(solid samples and/or samples with very short T2's) because it can obscure a substantial portion of the FID signal.

Another problem is the relatively low field stability of present FFC systems which causes considerable fluctuations in the tailing portions of FID's positioned far from its beginning and thus affects negatively the data for samples with long FIDs. To mitigate eliminate the this problem, one normally uses only the starting FID portions of the FIDs (typically covering the first 0.1 - 0.2 ms).

The shape of a simple, low-resolution FID is usually not suitable for discriminating between various sample magnetization components except, perhaps, in the co-presence of a very fast-decaying component and a very slow-decaying one.

The simplest data reduction algorithm for FIDs consists in averaging the magnitudes of the complex FID signal over e a data window positioned within its starting portion (Figure 26). The window can be freely positioned in a way to cut out any dead-time distortions and, at the same time, minimize field-fluctuation effects.

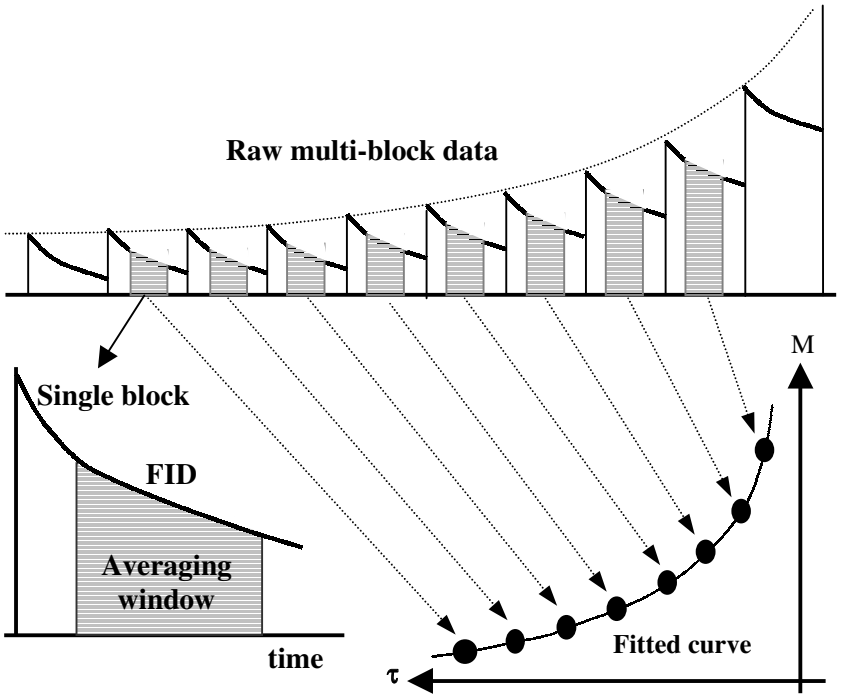

Figure 26. Example of the data reduction process.

Each data block of a multi-block sequence (in this case simple FIDs) is 'reduced' to a single value by means of averaging over a predefined data window and plotted against the block's τ-value. The resulting relaxation curve is than fitted to estimate its decay rate(s). The algorithm leaves a lot of freedom in setting the data window and including/excluding any number of initial or final blocks. Notice that in the PP case shown here, the τ-value decrease from left to right. This helps to minimize thermal variations of the magnet.

One of the advantages of window averaging is of course an additional S/N enhancement, which is roughly proportional to the square root of the number of data points present in the window (provided they are well reproducible). When too long portions of the FIDs are used, however, the S/N gain is eventually invalidated by FID signal fluctuations due to offset instabilities.

Published in **Advances in Inorganic Chemistry**, Vol. **57**, *Relaxometry of water-metal ion interactions*, Editors Rudi van Eldik R. and Ivano Bertini, Elsevier 2004 (ISBN 0-120-23657-5), pp.405-470.
This draft need not correspond to the final text. Reproduction is permitted for personal use only.

2. Spin echo

The classical Hahn-echo technique employs the basic sub-sequence 90_x-δ-180_y-δ'-Acq. It is applicable primarily to samples with long T_2 values (over 0.2 ms) in which it eliminates all dead-time problems, refocuses magnet inhomogeneity and enlarges by a factor of almost 2 the applicable data-reduction window which, in this case, should be centered over the top of the echo. When δ is longer than typical field- fluctuation times, spin echoes become sensitive to field instabilities. Consequently, the echo delay parameter δ must be kept small enough to avoid any field instability effects while, on the other hand, it should be long enough to make the top of the echo fall within the central part of the data -evaluation window (typical values are 0.05 - 0.1 ms). The second delay δ' needs to be long enough to cover the dead-time effects due to the second RF pulse but not necessarily longer (typical values are 0.01 - 0.02 ms).

It must be stressed that the spin-echo sequence is applied only during the detection period and its unique purpose is the estimate of the signal amplitude (in a sense, it is a replacement for the simple 90^o pulse). Consequently, in an arrayed multi-block experiment whose purpose is to measure $T_1(B_r)$, only the τ value is varied, while the delays δ and δ' are kept constant in order to make sure that no $T_2(B_A)$ effects leak into the experimental relaxation curves. Moreover, to avoid contamination of the echo by FID residues due to imprecise settings of RF pulses and to B1 inhomogeneity, proper phase cycling is highly recommended.

Spin-echo detection suppresses the sample magnetization components with short T_2 values (comparable to, or shorter than δ+δ'). Depending upon the context goal of the measurement, this can be either a disadvantage or an advantage. It makes sequences with spin-echo detection unsuitable for samples with very fast fast-decaying FIDs, such as those of rigid solids. On the other hand, it allows one to isolate the components with long $T_2(B_A)$ values (high mobility) from those with short $T_2(B_A)$ values (low mobility) in samples where such distinct components exist.

One should mention also the possibility of using the solid-echo sub-sequence of the type 90_x-δ-90_x-δ'-Acq (also known as quadrature echo). The principal purpose of this detection method is a reduction of the loss of signal due to the dead time. This makes it interesting for solid samples with strong dipolar interactions. One sets δ' just about long enough to suppress the dead time due to the second pulse. The value of δ, theoretically identical to δ', is adjusted so as to maximum maximize the amplitude of the resulting solid echo. Depending upon the structure of the sample, the echo can be substantially higher than a plain FID signal.

3. Multiple spin echoes

It is possible to use a whole series of 180^o pulses to repeatedly refocus the sample magnetization using the CPMG-like detection sub-sequence 90_x-$[δ\text{-}180_y\text{-}δ]_n$ with n anywhere between one and a few tens. Data acquisition can in this case proceed either all the time, starting almost immediately after the first RF pulse, or - more efficiently - in short segments centered around the top of each echo. When δ is smaller than typical field-fluctuation times, the train of RF pulses refocuses all field inhomogeneites and, due to its spin-locking properties, compensates quite efficiently any field instability.

The result is an enhancement of all the advantages of spin-echo detection. The number of usable data points in each acquired data array can in this case exceed that in an FID by a factor much larger than two. Since T_2 relaxation is going on during the detection, it is again important to keep δ rigorously constant during the whole multi-block experiment.

Published in **Advances in Inorganic Chemistry**, Vol. **57**, *Relaxometry of water-metal ion interactions*, Editors Rudi van Eldik R. and Ivano Bertini, Elsevier 2004 (ISBN 0-120-23657-5), pp.405-470.
This draft need not correspond to the final text. Reproduction is permitted for personal use only.

Like in the case of the single spin-echo detection, the multiple spin-echoes method attenuates magnetization components with short $T_2(B_A)$ values and the magnitude of the attenuation increases with increasing echo number - a fact which can be exploited for partial separation of sample components based on their $T_2(B_A)$ values.

4. CPMG echo train

An eEven more dramatic increase in S/N enhancement is achieved using a variety of the CPMG detection sub-sequence 90_x-[δ-180_y-δ-AcqS]$_n$ called LR-CPMG. This time, however, n is very large (for example, 1000) and each echo is sampled just once at the moment when it attains its maximum amplitude (this is the acquisition strobe AcqS). The result is an array of points describing the echo-tops envelope. When δ is kept very small (typically, one uses 0.05 ms), such envelope is completely insensitive to field inhomogeneity as well as - due to its excellent spin-locking performance - to field instabilities. One can, in fact, use the envelope to determine the value of $T_2(B_A)$, even though this is not the primary purpose of this detection sub-sequence in the present context.

Due to its excellent S/N enhancement properties, LR-CPMG detection is probably the only possible choice when the primary S/N ratio is very small. This regards in particular measurements of low-abundance nuclides and nuclides with low gyromagnetic ratio.

Like in the previous cases, the LR-CPMG sequence is applied exclusively during the detection period and its main purpose is again the estimate of the signal amplitude at the end of the relaxation period. However, the LR-CPMG envelope, whose data points are all quite insensitive to instrumental artifacts, can be analyzed by any of the standard methods in order to detect distinct components of sample magnetization on the basis of their $T_2(B_A)$ values. Having large arrays of data points, even the quasi-continuous Laplace inversion methods are easily applicable which paves the way for FFC investigations in complex multi-component systems.

A disadvantage of the LR-CPMG detection method is its total insensitivity to field/frequency offset which must be adjusted before a profile measurement and can not be corrected by means of a simple procedure during an automatic profile measurement. This requests a higher degree of long-term field stability (including any thermal effects) than the other methods. Despite the insensitivity of the technique, in fact, the field may not be allowed to drift too far from resonance where the RF pulses would loose their efficiency (excursions up to about 5 kHz are, however, quite tolerable).

5. Special detection techniques suppressing specific imperfections and artifacts

Once the acquisition field has been reached, the detection *sub-sequence*section of an FFC sequence is actually quite the same as in any other branch of NMR. This implies that the same categories of problems crop up and the same methods to solve them can be employed. Typical examples includeWe shall briefly mention two such cases.

i) Composite the use of *composite pulses to suppress B_1 inhomogeneity effects. (130) and*

The effects of B_1 inhomogeneity in various NMR sequences are well known and there is a number of ways to combat them. In FFC relaxometry, B_1 inhomogeneity is actually not much of a problem since it does not directly affect T_1 measurements. Whatever effect it has consists essentially in a loss of signal due to imperfect sample excitation and/or imperfect refocusing (in sequences using spin echoes and/or magnetization inversion).

Published in **Advances in Inorganic Chemistry**, Vol. **57**, *Relaxometry of water-metal ion interactions*, Editors Rudi van Eldik R. and Ivano Bertini, Elsevier 2004 (ISBN 0-120-23657-5), pp.405-470.
This draft need not correspond to the final text. Reproduction is permitted for personal use only.

The classical cure (*130*), consisting in the use of various composite pulses, is perfectly applicable also in FFC relaxometry.

The use of composite pulses is subject to several counter-indications, the principal of which is the fact that they last much longer than their simple prototypes. This makes their employment problematic in the case of rigid solids, as well as in detection sub-sequences which rely on extremely closely-spaced echoes.

In general, there is not much need for composite pulses in FFC relaxometry when the only purpose is fighting the inherent instrumental B_1 inhomogeneity. One usually delimits the sample height so as to make it fit inside the measurement coil, which is a less controversial way of reducing B_1 inhomogeneity than composite pulses. However, the employment of composite pulses is indicated in two cases:
- when the sample height simply cannot be reduced to fit inside the measurement coil, and
- when the sample itself induces a strong B_1 inhomogeneity.

The latter case is of interest, for example, when the sample contains metal particles (such as in some types of MRI relaxation contrast agents).

ii) and Signal signal detection sequences suppressing acoustic ringing. (131-132)

Acoustic ringing of the probe assembly after an RF pulse is a pesky problem which often limits the measurements of nuclides with low gyromagnetic ratios (it can also strongly interfere with measurements of samples containing piezoelectric components). The disturbance is often mis-interpreted as a particularly long dead-time disturbance, until one notices that, unlike normal dead-time components, it disappears when B_a is set to zero. It is difficult to remove because it follows the phase of the RF pulse and thus cannot be eliminated by any simple RF phase-cycling.

The classical cure (*131-132*), apart from special probe construction precautions, is a pulse sequence using a *phase & device* detection cycle in which one exploits the fact that acoustic ringing increases linearly with pulse width while NMR signal follows the sinusoidal nutation-angle curve. In its most elementary form, the cycle is composed of four steps (ideally with null δ):

Step 1)	0_x-δ-90_x-Acq (add)	introduces 90_x ringing
Step 2)	180_x-δ-90_x-Acq (subtract)	compensates 90_x ringing, introduces 180_x ringing
Step 3)	0_x-δ-90_{-x}-Acq (subtract)	introduces 90_{-x} ringing
Step 4)	180_x-δ-90_{-x}-Acq (add)	compensates 90_{-x} ringing, compensates 180_x ringing

Full anti-ringing quadrature cycle is a bit more complex, while extension of the anti-ringing pulse technique to signal detection sub-sequences other than the simple FID is quite simple.

XI. Advanced FFC sequences

So far we have discussed two different magnetization preparation methods (NP and PP) and several signal detection methods. The two aspects of an FFC sequence were so far independent of each other, thus giving rise to the full set of possible cross-combinations.

The original NP- and PP-type preparatory sub-sequences can be refined to partially compensate instrumental problems such as magnet heating during the measurements (see Section IV.D). The result are the so-called balanced NP and balanced PP preparatory sub-sequences.

Published in **Advances in Inorganic Chemistry**, Vol. **57**, *Relaxometry of water-metal ion interactions*,
Editors Rudi van Eldik R. and Ivano Bertini, Elsevier 2004 (ISBN 0-120-23657-5), pp.405-470.
This draft need not correspond to the final text. Reproduction is permitted for personal use only.

There are important FFC sequences in which the preparatory *sub-sequence*sections includes RF pulses. A typical example is the FFC version of the classical inversion recovery sequence (IR).

In some sequences, such as the FFC variety of the Jeener-Broekaert sequence, the RF pulses applied during the preparatory sub-sequence need to be coordinated in phase with those applied during the detection sub-sequence. In such cases the preparatory and detection *sub-sequence*sections of the FFC sequence are no longer mutually independent.

XI.A. Thermally balanced sequences

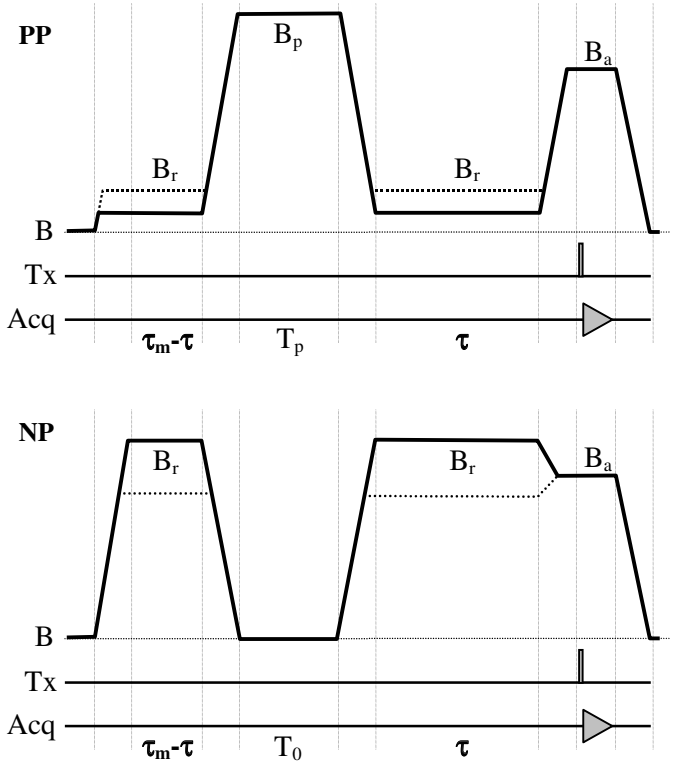

Fig. 27. **Thermally balanced PP and NP sequences**

PP) In the balanced PP sequence, the sample is first kept at the relaxation field B_r for a time τ_m-τ and, then pre-polarized at the polarization field B_p for a time T_p, and finally allowed to relax for time τ before the start of the detection period. The time T_p should be set to about $4T_1(B_p)$. As τ varies during a multi-block sequence, the polarization interval position moves horizontally but the total block duration and the mean power dissipation remain constant.
NP) The balanced non-polarized sequence is conceptually similar, except for the fact that the polarization interval is replaced by a magnetization annihilation interval in which the field is zero and whose duration should be about $4T_1(0)$.
In both cases, the time τ_m should be about or more than $4T_1(B_r)$. The concept can be combined with any detection mode, not just the simple FID detection shown here.

In a multi-block measurement sequence with interleaved phase cycle, there is a systematic, τ-dependent variation of the average magnet heating. In PP sequences with high B_p and small B_r, for example, the power dissipated on the magnet during each block increases with decreasing τ.

Published in **Advances in Inorganic Chemistry**, Vol. **57**, *Relaxometry of water-metal ion interactions*, Editors Rudi van Eldik R. and Ivano Bertini, Elsevier 2004 (ISBN 0-120-23657-5), pp.405-470.
This draft need not correspond to the final text. Reproduction is permitted for personal use only.

In the case of NP sequences with high B_r, the situation is inverted. Whichever is the case, the magnet temperature variations induce signal offset variations which, being correlated to with the τ values, could affect the relaxation curves.

The problem can been partially mitigated by hardware compensation devices (see Section IV.D). A complementary approach consists in setting up preparatory sequences which balance the average per-block thermal dissipation making it independent of τ. Though this does not remove the differences between the magnet temperature cycle within each block, it at least removes the systematic τ-dependent thermal drift.

The timing diagrams of the thermally balanced NP and PP sequences are shown in Figure 27. Comparing them with those of the corresponding unbalanced sequences, one notices immediately the price to be paid for the improved thermal performance consisting in an increased duration of each cycle (particularly those with small τ values) which makes the experiments longer by a factor of about 2.

Whether to use the balanced sequences or not thus becomes a matter of compromise. When magnet cooling is sufficiently efficient, all the used fields are far from maximum (keep in mind that heat dissipation on the magnet grows with the square of the field), and sensitivity is an issue, it may be advisable to use the unbalanced sequences and rely only on the hardware temperature compensation. Whenever the magnet is under a considerable thermal stress, however, it is advisable to use both the hardware compensation and the balanced sequences.

XI.B. Inversion Recovery

Figure 28 shows the diagram of the FFC version of the classical IR sequence. Notice that since the first RF pulse has to be applied at the acquisition field B_a because the probe is tuned to the Larmor frequency at that field. This implies the presence of an extra field-switching interval unless, of course, B_a equals B_p. For the IR preparatory sub-sequence, the latter condition represents an optimum (this goes hand-in-hand with the fact that a high acquisition frequency tends to improve the inherent S/N ratio). When $B_a = B_p$, the magnetization inversion is achieved by an RF pulse applied at the very end of the polarization interval.

In order to optimize the inversion, it is a good idea to make this pulse a composite one (except, maybe, in the case of rigid solid samples). As far as signal detection is concerned, all methods are acceptable so that, for example, IR preparation can be combined with a simple FID detection just as well as with the CPMG detection. Likewise, it is easy to combine IR with the balanced PP preparatory sub-sequence.

The IR-type sequences have a number of advantages, of which the two most important ones are:
a) Assuming ideal inversion and negligible switching-time effects, their relative magnetization variation turns out to be $\nu = (M_{max} - M_{min})/M_{max} = 1 + (B_r/B_p)$ which is always greater than 1 and, for $B_r \geq B_p$, reaches values $\nu \geq 2$. With respect to both NP- and PP-types of sequences, this amounts to better final precision due to an increased magnetization-variation range.
b) Since, unlike in the PP sequences, the factor ν never crosses zero, the IR sequences can be used throughout the full range of relaxation fields with no necessity of switching the sequence type at some particular relaxation field value. This makes the measurements of whole profiles internally more coherent.

Published in **Advances in Inorganic Chemistry**, Vol. **57**, *Relaxometry of water-metal ion interactions*,
Editors Rudi van Eldik R. and Ivano Bertini, Elsevier 2004 (ISBN 0-120-23657-5), pp.405-470.
This draft need not correspond to the final text. Reproduction is permitted for personal use only.

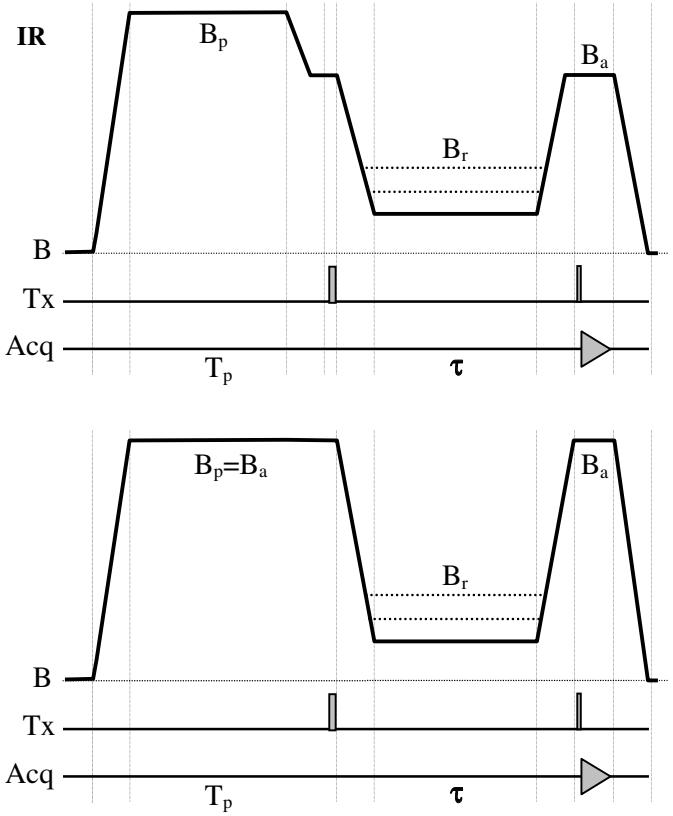

Fig. 28. **FFC Inversion Recovery sequence.**

In the upper case the sample is first pre-polarized in a filed B_p, then switched to the 'acquisition' field B_a where the first RF pulse of 180° is applied and the sample magnetization is inverted. The field is then switched to B_r and the sample is allowed to relax for the variable time τ. Finally, the field is switched again to the acquisition value and the magnetization is sampled by any of the sample-detection method (here a simple FID following a 90° RF pulse). Notice that, as shown in the lower diagram, in the special case when B_p=B_a it is possible to neatly avoid the extra switching interval prior to the inversion pulse.

XI.C. Jeener-Broekaert dipolar- order relaxation sequence

The classical Jeener-Broekaert sequence (*133*) is used to determine the dipolar-order relaxation time T_{1D} (in systems of spin 1/2 nuclids) and the T_{1Q} relaxation time (in systems with spin 1 nuclides)of spin 1 nuclides with quadrupolar contributions to T_1. Its FFC version is similar to the Inversion Recovery, except that the first 180° pulse is replaced by the sequence 90_y-δ-45_x, the detection pulse becomes 45_x and a special phase cycle is required. We shall not dwell on the details and purpose of the sequence since they go beyond the scope of this paperChapter. We wish to underline, however, the fact that sequences of this type require a close coordination of the preparatory sub-sequence with the signal-detection sub-sequence in order to isolate not just a particular magnetization component but a particular relaxation pathway.

Published in **Advances in Inorganic Chemistry**, Vol. **57**, *Relaxometry of water-metal ion interactions*, Editors Rudi van Eldik R. and Ivano Bertini, Elsevier 2004 (ISBN 0-120-23657-5), pp.405-470.
This draft need not correspond to the final text. Reproduction is permitted for personal use only.

XII. Conclusions and perspectives

The instruments currently produced by Stelar prove that Fast-field-cycling NMR relaxometry instrumentation is industrially viable in the sense that i) its specifications are reasonably reproducible and ii) once installed, the reliability of the instruments is comparable to that of any other NMR equipment. The overall performance, unthinkable-of only a few years ago, is best witnessed by the examples shown in Figure 29.

This, by itself, might be considered as a nice achievementaccomplishment. However, the instrumentation is at present still very far from the underlying utopisticutopist ideal represented by a hypothetical system with a maximum field in excess of 10 T, high-resolution-grade field homogeneity and stability, and switching times of the order of just a few microseconds.

A more realistic near-future evolution shall certainly include the following steps, some of which are already under development:

- Further increase of the maximum field beyond the present limit of about 1T.
- Implementation of efficient devices for the compensation of environmental magnetic fields, both stationary and variable/alternating and a push toward more reliable measurements in the relaxation-field region of 100 Hz- 10 kHz.
- Progressive improvements of the system stability and reproducibility.
- Refinements of magnet technology in order to achieve better field homogeneity.
- Use of double-irradiation methods for the exploration of cross-relaxation phenomena.
- Novel approaches to the study of relaxation dynamics in complex systems (sequences, etc).
- A drive towards *high-resolution variable-field FFC NMR relaxometry* (HR-FFC-NMRD), possibly combining the respective advantages of the FFC and the sample-shuttling methods.

Much shall depend upon the development of the many potential application fields. Though, from the chemical point of view, FFC is still a low-resolution NMR technique, it has already proved itself as an excellent research tool in many application fields areas such as the study of contrast agents (134-141), dynamics of proteins (142-153), polymers (154-162) and liquid crystals (163-168), dynamics of water in rocks and cements (169-176), etc.

The increasing interest in FFC NMR relaxometry is also evidenced by the fact that there had have been in recent years several international conferences in recent years specifically dedicated to the method. Even so, there are still many untapped application areas and additional ones shall come to frontup with further developments of the technology. Opening such novel fields shall undoubtedly provide a strong feedback and novel challenges to FFC NMR engineering .

Published in **Advances in Inorganic Chemistry**, Vol. **57**, *Relaxometry of water-metal ion interactions*, Editors Rudi van Eldik R. and Ivano Bertini, Elsevier 2004 (ISBN 0-120-23657-5), pp.405-470.
This draft need not correspond to the final text. Reproduction is permitted for personal use only.

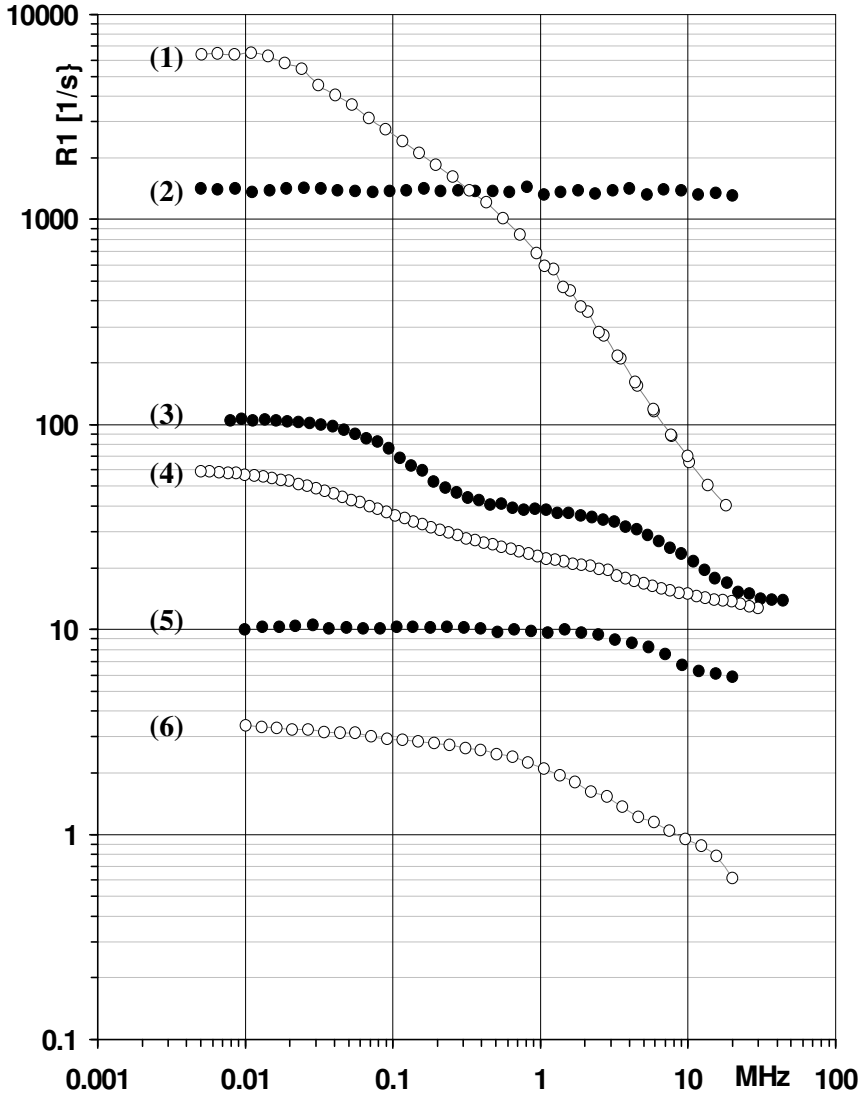

Fig. 29. **Examples of FFC NMRD profiles.**

All NMRD profiles shown here were measured with the Stelar FFC NMR Relaxometer at 25°C using the automated profile acquisition Wizard. The observed nuclide was ^{1}H in all cases except (5) where it was ^{2}D. The individual curves show: **(1)** Parafilm M (American National Can Co.), **(2)** 2.1M $Dy(ClO_4)_3$ in H_2O (courtesy Dr.L.Holm), **(3)** 2mM $MnCl_2$ in H_2O, **(4)** egg yolk, (**5**) 10 mM Gd^{3+} in D_2O, **(6)** egg albumen.

Published in **Advances in Inorganic Chemistry**, Vol. **57**, *Relaxometry of water-metal ion interactions*, Editors Rudi van Eldik R. and Ivano Bertini, Elsevier 2004 (ISBN 0-120-23657-5), pp.405-470.
This draft need not correspond to the final text. Reproduction is permitted for personal use only.

References

(1) Broer, L.J.F. *Physica* **1943**, *10*, 801.
(2) Torrey, H.C. *Phys.Rev.* **1946**, *69*, 680.
(3) Pound, R.V.; Purcell, E.M.; Torrey, H.C. *Phys.Rev.* **1946**, *69*, 681.
(4) Bloch, F. *Phys.Rev.* **1946**, *70*, 460.
(5) Bloch, F.; Hansen, W.W.; Packard, M.E. *Phys.Rev.* **1946**, *70*, 474.
(6) Bloembergen, N. "Nuclear Magnetic Relaxation",
The Hague Martinns: Nijhoff 1948, reprinted by Benjamin: New York 1961.
(7) Bloembergen, N.; Purcell, E.M.; Pound, R.V. *Phys.Rev.* **1948**, *73*, 679.
(8) Drain, L.E. *Proc.Roy.Soc.(London)* **1949**, *A62*, 301.
(9) Torrey, H.C. *Phys.Rev.* **1949**, *76*, 1059.
(10) Wright, A. *Phys.Rev.* **1949**, *76*, 1826.
(11) Bloch, F.; Hansen, W.W.; Packard, M.E. *Phys.Rev.* **1946**, *69*, 680.
(12) Purcell, E.M.; Torrey, H.C.; Pound, R.V. *Phys.Rev*. **1946**, *69*, 36.
(13) Gorter, C.J. *Physica* **1936**, *3*, 995.
(14) Gorter, C.J.; Broer, L.J.F. *Physica* **1942**, *9*, 591.
(15) Ramsey, N.F.; Pound, R.V. *Phys.Rev.* **1950**, *77*, 278.
(16) Pound, R.V. *Phys.Rev.* **1951**, *81*, 156.
(17) Abragam, A. "The Principles of Nuclear Magnetism", Clarendon Press: Oxford 1961.
(18) Kubo, R.; Tomita, K. *J.Phys.Soc.Japan.* **1954**, *9*, 888.
(19) Kubo, R. *J.Phys.Soc.Japan.* **1954**, *9*, 935.
(20) Torrey, H.C. *Phys.Rev.* **1953**, ***92***, 962.
(21) Koster, G.F.; Slater, J.C. *Phys.Rev.* **1954**, *95*, 1167.
(22) Redfield, A.G. *IBM J.Res.Develop.* **1957**, *1*,19.
(23) Bloch, F. *Phys.Rev.* **1957**, *105*,1206.
(24) Argyres, P.N.; Kelley, P.L. *Phys.Rev.* **1964**, *134*, A98.
(25) Solomon, I. *Phys.Rev.* **1955**, *99*, 559.
(26) Hubbard, P.S. *Phys.Rev.* **1958**, *109*, 1153.
(27) Bloembergen, N.; Shapiro, S.; Pershan, P.S.; Artman, J.O. *Phys.Rev.* **1959**, *114*, 445.
(28) Gutowsky, H.S.; Lawrenson, I.J.; Shimomura, K. *Phys.Rev.* **1961**, *6*, 349.
(29) Shimizu, H. *J.Chem.Phys.* **1962**, *37*,765.
(30) Ter Haar, Ed. "Fluctuation, Relaxation and Resonance in Magnetic Systems",
Oliver and Boyd: Edingurgh 1962.
(31) Hubbard, P.S. *Phys.Rev.* **1962**, *128*, 650 and **1963**, *131*, 275
(32) Tomita, K.; Tanaka, M. *Progr.Theor.Phys.(Kyoto)* **1963**, *29*, 528 and **1963**, 29, 651.
(33) Runnels, L.K. *Phys.Rev.* **1964**, 134A, 28.
(34) Hilt, R.L.; Hubbard, P.S. *Phys.Rev.* **1964**, *134A*, 392.
(35) Redfield, A.G., in "Advances in Magnetic Resonance", Waugh J. Ed., Academic Press 1965, Vol.1.
(36) Bonera, G., Rigamonti, A. *J.Chem.Phys.* **1965**, *42*, 171 and **1965**, *42*, 175.
(37) Noggle, J.H. *J.Chem.Phys.* **1965**, *43*, 3304.
(38) Gordon, R.G. *J.Chem.Phys.* **1966**, *44*, 228; **1966**, *44*, 1184 and **1966**, *45*, 1635.
(39) Blicharski, J.S. *Phys.Letters* **1967**, *24A*, 608.
(40) Huntress, W.T.Jr. In "Advances in Magnetic Resonance", Waugh, J.; Ed., Academic Press 1967, Vol.3.
(41) Gordon, R.G. In "Advances in Magnetic Resonance", Waugh, J.; Ed., Academic Press 1968, Vol.4.
(42) Blicharski, J.S. *Acta Phys.Polonica* **1969**, *36*, 211; **1970**, *A38*, 19 and **1970**, *A38*, 25.
(43) Hubbard, P.S. *J.Chem.Phys.* **1969**, *51*, 1647.
(44) McBrierty, V.J.; Douglas, D.C. *J.Magn.Resonance* **1970**, *2*, 352.
(45) Ivanov, E.N. *Phys.Status Solidi (Germany)* **1970**, *42*, 453.
(46) Sykora, S. *J.Chem.Phys.* **1970**, *52*, 4818 and **1971**, *54*, 2469.
(47) Hubbard, P.S. *J.Chem.Phys.* **1970**, *52*, 563.
(48) Noack, F. In "NMR-Basic Principles and Progress",
Diehl, P.; Fluck, E.; Kosfeld, R; Eds. Springer Verlag 1971, Vol.3.
(49) Béné, G.J. *Physics Reports* **1980**, *58*, 213.
(50) Abragam, A.; Proctor, W.G. *Phys.Rev.* **1958**,*109*, 1441.

Published in **Advances in Inorganic Chemistry**, Vol. **57**, *Relaxometry of water-metal ion interactions*,
Editors Rudi van Eldik R. and Ivano Bertini, Elsevier 2004 (ISBN 0-120-23657-5), pp.405-470.

This draft need not correspond to the final text. Reproduction is permitted for personal use only.

(51) Schumacher, R.T. *Phys.Rev.* **1958**, *112*, 837.
(52) Pershan, P.S. *Phys.Rev.* **1960**, *117*, 109.
(53) Pfeifer, H. *Z.Naturforsh.* **1962**, *17a*, 279.
(54) Hauser, R.; Noack, F. *Z.Phys.* **1964**, *182*, 93.
(55) Johnson, B.C.; Goldburg, W.I. *Phys.Rev.* **1966**, *145*, 380.
(56) Sprinz, H. *Ann.Phys.* **1967**, *20*, 168.
(57) Hauser, R.; Kolb, H.; Siegle, G. *Z.Angew.Phys.* **1967**, *22*, 375.
(58) Koenig, S.H.; Shillinger, W.E. *J.Biol.Chem.* **1968**, *244*, 3283 and **1969**, *244*, 6520.
(59) Jones, G.P.; Daycock, J.T.; Roberts, T.T. *J.Phys.E (Sci.Instr.)* **1968**, *2*, 630.
(60) Florkowski, Z.; Hennel, J.W.; Blicharska, B. *Nucleonica* **1969**, *14*, 563.
(61) Kimmich, R.; Noack, F. *A.Angew.Phys.* **1970**, *29*, 248.
(62) Blinc R.; Luzar,M.; Mali,M.; Osredkar, R.; Seliger, J.; Vilfan, M. *J.Physique Colloque* **1976**, *37*, *C*3.
(63) Edmonts, D.T. *Phys.Rep.* **1977**, *29*, 233.
(64) Thayer, A.M.; Pines, A.; *Acc. Chem. Res.* **1987**,20,47
(65) Noack, F. In "Progress in NMR Spectroscopy",
Emsley, J.W.; Feeney, J.; Sutcliffe, L.H.; Eds. Pergamon Press **1986**, Vol.18.
(66) Koenig, S.H.; Brown, R.D. In "Progress in NMR Spectroscopy",
Emsley, J.W.; Feeney, J.; Sutcliffe, L.H.; Eds. Pergamon Press 1990, Vol.22.
(67) Schweikert, K.H; Krieg, R.; Noack, F. *J.Magn.Reson.* **1988**, *78*, 77.
(68) Hoult, D.I.; Richards, R.E. J.Magn.Reson. **1976**, *24*, 71.
(69) Sykora, S. *Magn.Reson.Imaging* **1991**, *9*, 833.
(70) Anoardo, E.; Ferrante, G.M.; *Appl.Magn. Reson.* **2003,** 24, 85-96.
(71) Kroon, D.J.; "*laboratory Magnets" Philips technical library* –**1968**
(72) Anoardo, E.;Galli, G.; Ferrante, G.M. *Appl.Magn. Reson.* **2001,** 20, 365-404
(73) Grössl, G.; Winter, F.; Kimmich, R. *J. Phys* **1985** E 18, 358
(74) Packard, M.; Varian, R. *Phys. Rev.* **1954**, 93, 941
(75) Redfield, A.; Fite, W. *Bleich Rev. Sci. Instrum.* **1968** 39, 710
(76) Kimmich, R. *Bul. Magn. Reson.* **1980** 1, 195
(77) Seitter R.-O., Kimmich R. in *Encyclopedia of Spectroscopy and Spectrometry*
(Lindon J. C. Tranter G. E., Holmes J. L. Eds.), 2000-2008, London. Academic Press, 1999.
(78) Brown, R.D.; Koenig S.H., **1977** IBM research Rep. RC6712, Yorktown Heights
(79) Westphal,W. *Handbuch der Physik Bd. XV (Magnetismus/Elektromagnetisches Feld)* 1927.
(80) Hart, P.J. *Universal Tables for Magnetic Fields of Filamentary and Distributed Circular Currents* 1967.
(81) Kohlrausch, F. *Praktische Physik Bd.* II 1968.
(82) Eder, F.X. *Moderne M e methoden der Physik Bd. II* 1972.
(83) Schnell, G. *Magnete,Grundlagen,Aufbau,Anwendungen*. 1973.
(84) Neuman, H. *Archiv für Technisches Messen* 1940.
(85) Garret, M.W. *J.Appl.Phys*. **1951**,22,1091, **1967**,38,2563 and **1969**,20,3171.
(86) Saint-Jalmes, H.; Taquin, J. *Rev.Sci.Instrum.* **1981**,52,1501.
(87) Ruark, A.E.; Peters,M.F. *J.Opt.Soc.Am.* **1926**,131,205
(88) Fanselau, G. *Z.Phys.* **1936**,54,260
(89) McKeehan, L.W. *Rev.Sci.Instrum.* **1936**,7,150
(90) Hak, J. *Arch.Elektrotech.* **1936**,30,736
(91) Montgomery, D.B. *Solenoid Magnet Design*. **1969**
(92) Cesnak, L.; Kabat, D. *J.Phys.* **1972**,5,944
(93) Reményi, G.; Kirchner, I. ; Poiuesz, T. *Cryogenics* **1977**,17,565
(94) Grössl, G. ; Winter, F. ; Kimmich, R. *J.Phys.E.(Sci.Instr.)* **1985**,18,538
(95) Gaume, F. In "High Magnetic Fields", Kolm,H.; Lax, B.; Bitter, F.; Mills, R.; Eds. Wiley New York 1962.
(96) Hart, P.J. In "Universal Tables for Magnetic Fields of Filamentary and Distributed Circular Currents"
Elsevier New York 1967.
(97) Schnell, G. In "Magnets: Basic Relations, Engineering, Applications", Thiemig, K.; Munich 1973.
(98) Pucell, E.M.; Pound, R.V. *Phys.Rev.* **1950**, *77*, 279.
(99) Hahn, E.L. *Phys.Rev.* 1950, *80*, 580.
(100) Carr, H.Y; Purcell, E.M.; *Phys.Rev.* **1954**, *94*, 630.
(101) Meiboom, S.; Gill, D. Rev.Sci.Instrum. **1958**, *29*, 688.
(102) Powles, J.G.; Mansfield, P. *Phys.Letters* 1962, *2*, 58. Solid echo

Published in **Advances in Inorganic Chemistry**, Vol. **57**, *Relaxometry of water-metal ion interactions*,
Editors Rudi van Eldik R. and Ivano Bertini, Elsevier 2004 (ISBN 0-120-23657-5), pp.405-470.
This draft need not correspond to the final text. Reproduction is permitted for personal use only.

(103) Slichter, C.P. "Principles of Magnetic Resonance",
Harper & Row: New York 1963; 2nd edition Springer-Verlag: New York 1978.
(104) Freeman R, Wittekoek S. Colloque Ampère **1969**, *XV*, 205.
(105) Farrar, T.C.; Becker, E.D. "Pulse and Fourier Transform NMR", Academic Press: New York 1971.
(106) Fukushima, E.; Roeder, S.B.W. "Experimental Pulse NMR. A Nuts and Bolts Approach",
Addison-Wesley: New York 1981.
(107) Gerstein, B.C.; Dybowski, C.R. "Transient Techniques in NMR of solids", Academic Press: London 1985.
(108) Freeman, R. "Nuclear Magnetic Resonance", Longman 1987.
(109) Homans, S.W. "A Dictionary of NMR Concepts", Oxford University Press: Oxford 1989.
(110) Kimmich, R. "NMR Tomography, Diffusometry, Relaxometry", Springer-Verlag: Berlin 1997.
(111) Ernst, R.R.; Bodenhausen, G.; Wokaun, A.
"Principles of Nuclear Magnetic Resonance in One and Two Dimensions", Clarendon Press: Oxford 1987.
(112) Atta-ur-Rahman, "One and Two Dimensional NMR Spectroscopy", Elsevier: Amsterdam 1989.
(113) Bonera, G.; Paolucci, G.; Ruffato, C.; Sykora, S. "Risonanza Magnetica Nucleare in Medicina",
Piccin Nuova Libreria: Padova 1984.
(114) Ernst, R.R. *Quarterly Reviews of Biophysics* **1987**, *19*,183.
(115) Haacke, E.M.; Brown, R.W.; Thomson, M.R.; Venkatesan, R.
"Magnetic Resonance Imaging. Physical Principles and Sequence Design", Wiley-Liss 1999.
(116) Zhi-Pei, L.; Lauterbur, P.C. "Principles of Magnetic Resonance Imaging", IEEE Press 2000.
(117) Stilbs, P. In "Progress in NMR Spectroscopy",
Emsley, J.W.; Feeney, J.; Sutcliffe, L.H., Eds. Pergamon Press 1987, Vol 19.
(118) Lindon, J.C.; Ferrige, A.G. In "Progress in NMR Spectroscopy",
Emsley, J.W.; Feeney, J.; Sutcliffe, L.H., Pergamon Press 1980, Vol.14.
(119) Brown, R.J.S. *J.Magn.Reson.* **1989**, *82*, 539.
(120) Clayden, N.J.; Hesler, B.D. *J.Magn.Reson.* **1992**, *98*, 271.
(121) Lin, Y.Y.; Ge, N.H.; Hwang, L.P. *J.Magn.Reson.* **1993**, *A105*, 65.
(122) Jakes, J. *Czech.J.Phys.* **1993**, *B43*, 1.
(123) Lupu, M.;Todor, D. *Chemometrics and Intelligent Lab.Systems* **1995**, *29*, 11.
(124) Borgia, G.C.; Brown, R.J.S.; Fantazzini, P. *J.Magn.Reson.* **1998**, *132*, 65.
(125) Borgia, G.C.; Brown, R.J.S.; Fantazzini, P. *Magn.Reson.Imaging* **1998**, *16*, 549.
(126) Borgia, G.C.; Brown, R.J.S.; Fantazzini, P. *J.Magn.Reson.* **2000**, *147*, 273.
(127) Borgia, G.C.; Brown, R.J.S.; Fantazzini P. *Magn.Reson.Imaging* **2001**, *19*, 473.
(128) Song, Y.Q.; Venkataramanan, L.; Huerlimann, M.D.; Flaum, M.; Frulla, P.; Straley, C.
J.Magn.Reson. **2002**, *154*, 261.
(129) Weiss, G.H.; Ferretti, J.A. In "Progress in NMR Spectroscopy",
Emsley, J.W.; Feeney, J.; Sutcliffe, L.H.; Eds., Pergamon Press 1988, Vol 20.
(130) Levitt, M.H. In "Progress in NMR Spectroscopy",
Emsley, J.W.; Feeney, J.; Sutcliffe, L.H.; Eds., Pergamon Press 1986, Vol 18.
(131) Patt, S.L. *J.Magn.Reson.* 1982, *49*,161.
(132) Gerothanassis, I.P. In "Progress in NMR Spectroscopy",
Emsley, J.W.; Feeney, J.; Sutcliffe, L.H.; Eds., Pergamon Press 1987, Vol 19.
(133) Jeener, J.; Broekaert P. *Phys.Rev.* **1967**, *157*, 232.
(134) Aime, S;Botta, M;Fasano, M; Terreno, M. Chem. Soc. Rev. **1998**, 27, 19
(135) Aime, S. Angew. Chem. Int. Ed. **2000**, 39, 747
(136) Muller, R.N; Raduchel, B.; Laurent, S; Platzek, J.; et al., Eur. J. Inorg. Chem. **1999,** 1949-1955
(137) Toth, E.; Connac, F.; Helm, L.; Adzamli, K.; Merbach A., Eur. J. Inorg. Chem., **1988,** pp 2017
(138) Gossuin, Y.; Roch, A.; Lo Bue, F.; Muller, R.; Gillis P. Magn. Reson. Med., **2001**, **46(3)**, 476-81.
(139) Roch, A.;Muller, R.; Gillis, P.; J. Magn. Reson. Imaging. **2001** 14(1), 94-6.
(140) Corsi, DM.; Vander Elst, V.; Muller, RN.; et al, J.A.Chemistry. **2001**, Apr 1; 7(7), 1383-9.
(141) Comblin, V.; Gilsoul, D.; Hermann, M.; et al, Coord. Chem. Rev. **1999**, 185-186, pp 451.
(142) Bertini, I.; Luchinat, C. Coord. Chem. Rev. **1996,** 150, 1. 1996
(143) Bertini, I.; Luchinat, C.; Brown, R.D.; Koenig S.H. J. Am. Chem. Soc., **1989** 111, 3532-3536
(144) Koenig, S.H.; Schillinger W.E.; J.Biol. Chem., **1969** 244, 3283-3289.
(145) Banci, L.; Bertini, I.; Hallewell, R.A.; Luchinat, C.; Viezzoli M.S.; Eur. J. Biochem., **1989,** 184, 125-129
(146) Kimmich, R.; Noack, F.; Z. Naturforsch. **1970,** 25a, 299 - 301
(147) Kimmich, R.; Noack, F.; Z. Naturforsch. **1970**, 25a 1680 - 1684

Published in **Advances in Inorganic Chemistry**, Vol. **57**, *Relaxometry of water-metal ion interactions*,
Editors Rudi van Eldik R. and Ivano Bertini, Elsevier 2004 (ISBN 0-120-23657-5), pp.405-470.
This draft need not correspond to the final text. Reproduction is permitted for personal use only.

(148) Kimmich, R., Naturforsch, Z.; **1971,** 26b, 1168 – 1170
(149) Kimmich, R., Makromol. Chem., Macromol. Symp. **1990,** 34, 237 - 248
(150) Korb, J.P.; Bryant, R.G., Magn. Reson. Med. **2002,** 48, 21.
(151) Korb, J.P.; Bryant, R.G., J. Chem. Phys. **2001,** 115, 10964.
(152) Korb, J.P.; Van-Quynh, A.; Bryant, R.G.; **Chem. Phys. Letters 2001** 339, 77.
(153) R. Kimmich, "Encyclopedia of Nuclear Magnetic Resonance",
John Wiley Ltd, Chichester, **1996**, Vol. 5, 3083 - 3088
(154) Bryant R.G.; Brown, R.D.; Koenig S.H., Biophys. Chem. **1982** 16, 133-137 ()
(155) Halle, B.; Denisov, V.P.; Venu K.; Biological Magnetic Resonance.
1999, Vol. **17**, New York: Kluwer-Plenum.
(156) Kimmich, R.; Winter, F.; Progr. Colloid & Polymer Sci. **1985**, 71,66 - 70
(157) Kimmich, R.;Winter, F.;Nusser, W.;Spohn, K.-H., J. Magn. Resonance **1986,** 68 263 – 282
(158) Zeumer U.; Dippel, T.; Noack F.; et al, J. Chem. Phys., **1992**, 97, 3794.
(159) Voigt, G.; Kimmich R.Polymer,**1980,** 21, 1001.
(160) Koch, H.; Bachus, R.; Kimmich, R. Polymer **1980,** 21, 1009.
(161) Stapf, S.; Kimmich, R., Macromolecules, **1996,** 29,1638 - 1641
(162) Kimmich, R. Polymer **1975**, 16, 851 – 852.
(163) Noack F.; Schweikert K.H. Molecular Dynamics in Liquid Crystals,
ed. by G.R.Luckhurst and C.A. Veracini. Kluver Academic Publications, London 1994. p. 233
(164) Struppe, J.; Noack, F.; Klose G., Z. Naturforsch **1997,** A 52, 681-694.
(165) Ribeiro, A.C.; Sebastiao, P.J.; Vilfan, M., Liq. Cryst. **1988**, 3, 937-945.
(166) Anoardo, E.; Pusiol D., Phys. Rev. Lett. **1996** 76, 3983-3986.
(167) Burnell, E.E.; Capitani, D.; Casieri C.; Segre A.L., J. Phys. Chem. **2000,** B104, 8782.
(168) Stapf, S.; Kimmich, R. Mol. Physics **1997,** 92, 1051-1060.
(169) Korb J.P.; Hodges M.W.; Bryant R., G.Phy. Rev. E., **1997,** 56(2), 1934-1945.
(170) Stapf, S.; Kimmich R.; Nieß, J., J. Appl. Phys., **1994**, 75(1), 529-537.
(171) Stapf, S.; Kimmich, R.; Seitter R.O. Phys. Rev. Lett., **1995** 75, 2855.
(172) Korb, J.P.; Hodges, M.W.; Gobron, T.; Bryant, R.G. Phy. Rev. E., **1999,** 60(3), 3097-3106.
(173) Levitz, P.; Korb, J.P.; Bryant, R.G., J. Chem. Phys, **1999**, 96, 1494-1505.
(174) J.-P. Korb, J.P.; Whaley, M;. Bryant, R.G., Phys. Rev. **1997** E 56, 1934-1945.
(175) Barberon; Korb, J.-P.; Petit, D.; Morin, V.; Bermenjo, E., Phys. Rev. Letters, **2003**, 90, 116103.
(176) Porteneuve, C.; Korb, J,-P.; Petit, D.; Zanni, H., Cement and Concrete Research, **2002**, 32, 97.

Published in **Advances in Inorganic Chemistry**, Vol. **57**, *Relaxometry of water-metal ion interactions*,
Editors Rudi van Eldik R. and Ivano Bertini, Elsevier 2004 (ISBN 0-120-23657-5), pp.405-470.
This draft need not correspond to the final text. Reproduction is permitted for personal use only.